Groundwater Flooding of Superficial Gravels in an Urbanized Catchment

Jonathan D. Paul*, Aneena Ajmi, Doris Bolaji-Dada, Samuel Bordessoule
Royal Holloway, University of London, Egham, TW20 0EX, UK
*Corresponding author: J.D. Paul (jonathan.paul@rhul.ac.uk)

This paper is a non-peer reviewed preprint submitted to EarthArXiv. It has been submitted to Journal of Flood Risk Management *for peer review (December 2024).*

Key Points:

- Investigation of groundwater disposition and emergence in urbanized, highly permeable River Terrace Gravel aquifer, southern UK
- Joint hydrologic, geophysical, laboratory, citizen science approach in early January 2024
- Dramatic hydraulic gradients and fast flow pathways suggest urbanization dominates groundwater flooding, rather than elevation or river stage

Abstract

Groundwater behavior in superficial gravel aquifers is globallypoorly understood, especially across urban regions where drinking water is sourced from elsewhere. We focus on one such region around Staines, SE UK, where local River Terrace Gravels form a thin (<10 m) superficial aquifer. Our objective was to explain the unusually broad and long-lived distribution of flooding by investigating local groundwater level fluctuations and flow. Over a period in January 2024, we instigated a targeted citizen science program to leverage local knowledge of floodwater, which was determined to match groundwater chemistry. We designed geophysical surveys (ground-penetrating radar and seismic refraction) to produce high-resolution water table maps, validated against well measurements. Flow rates and hydraulic conductivity, K, of the gravels were determined both in the field (via pumping and tracer tests) and laboratory, to obviate any scale effects. K depended non-linearly on hydraulic gradient, with Darcyan behaviour breaking down at low (<0.03) gradients, in conditions approaching turbulent flow. Dramatic, localized fluctuations in groundwater level, combined with the existence of several fast-flow pathways, are explained by the strong heterogeneity of the gravels, as well as their sensitivity to the imposition of sub-surface obstacles such as clay-lined backfilled gravel pits, or deep basements. These manifestations of urbanization drive observed patterns of groundwater emergence, together with aquifer thickness, rather than changes in river stage or surface elevation alone. Our experience motivates us to suggest that groundwater flooding be considered as significant as fluvial flooding in the production of risk maps by environmental regulatory bodies.

Plain Language Summary

We worked with local residents to define areas of flood risk for a region of the River Thames floodplain in the southern UK. However, this flooding, while intense, is not due to rivers: instead, water rises up from the ground, leading to highly localized patches of groundwater flooding in basements and on roads. We sought to investigate the pattern of this flooding by first trying to understand how water flowed through the local gravel substrate. We conducted several field surveys and laboratory analyses to demonstrate that the depth to water under the surface varies greatly over very short distances, and that sub-surface water flow is rapid and complicated. The gravels are a highly porous aquifer that is sensitive to any human-imposed disturbance, like excavations or deep basements. We suggest that patterns of urbanization dictate observed flooding – far more so than proximity to surface drainage – and that environmental regulators in urbanized catchments across the globe should consider groundwater as explicitly as river water when generating models of future flood risk.

1 Introduction

1.1 Groundwater Flooding

The impacts of groundwater emergence at the surface can be difficult to distinguish yet severe – especially in urban areas with extensive sub-surface infrastructure – including basement and tunnel flooding, ground heave, and overwhelming the capacity of foul drainage systems (Macdonald et al., 2008). However, these impacts are often poorly understood, constrained, and mapped, relative to fluvial flood forecasting and management (Parkin, 2024). The focus of this paper is groundwater flooding in an urban area that is located on the floodplain of the River Thames, UK, underlain by highly permeable river terrace gravels (Section 1.2).

Relatively little is known about groundwater (relative to fluvial) flood risk (Morris et al., 2007). The UK regulator for flood risk management, the Environment Agency, is limited in its remit to events that pertain to “rivers and the sea” (EA, 2020). Risk is related to recurrence interval (e.g. a 1 in 100-year event is assigned “medium risk”), which in turn is calculated based on known historical flood extents, topography, fluvial geomorphology, and river stage and flow time series. The UK Department for Environment and Rural Affairs (Defra) only recently commenced a scoping study aimed at producing a set of provisional groundwater emergence risk maps, based on low spatial resolution (>10 km^2) hydrogeological observables including transmissivity and storage of known major aquifers (Defra, 2020).

Yet the resolution of these maps is not the only outstanding challenge. The hydrogeology of floodplains is typically highly heterogeneous, which influences catchment water flows together with the complex interactions between surface water and groundwater; but it is often simplified or overlooked (Dochartaigh et al., 2019). The hydraulic connection between an aquifer an a major river is often strong, leading to rapid groundwater level rise and recession over a matter of hours; but sub-surface infrastructure such as sheet piling and deep, impermeable basements weakens this coupling, retarding groundwater level rise and maintaining high heads over several weeks in cities including London and Paris (Ding et al., 2008; Dochartaigh et al., 2019).

Moreover, climate change and population growth – leading to increased construction and sub-surface engineering across floodplains – have led to more frequent extreme groundwater flooding, such as that experienced across southern England in the winter of 2013/14, causing £144M in insured losses (Fan, 2024).

Macdonald et al. (2012) investigated groundwater flooding in the city of Oxford, noting the significant contribution of groundwater to river flow during summer, and recharge of the flood plain sediments from the effluent River Thames in winter. They quantified flood risk (rather than susceptibility), which was directly linked to changes in surface elevation resulting from urbanization. The duration of groundwater flood events was shown to directly reflect aquifer transmissivity, with the superficial river terrace gravels at Oxford yielding "flashy" groundwater emergence behavior relative to other areas of southern England underlain by chalk (Macdonald et al., 2012; Robins and Finch, 2012). McKenzie et al. (2012) conducted a UK-wide assessment of groundwater flood susceptibility, based on a 90 m-resolution Digital Elevation Model and comparatively sparse hydrogeological data, but this assessment was not validated against areas of known groundwater emergence, and did not include local complexities such as "groundwater-induced floods" (i.e. surface discharge via bourne springs and highly permeable shallow horizons: Robins and Finch, 2012).

1.2 Study Area: Gravel Hydrology

This study considered the area around Staines, a mid-sized (20,000 people) commuter town ~30 km W of London in SE UK, which is bisected by the River Thames and sits in the center of a broad floodplain, with the entirety of the Roman core of the town at 14–16 m above sea level (Figure 1a). The hydrogeology of the Thames Basin has been dealt with extensively elsewhere (e.g. Ellison et al., 2004). Briefly: two distinct groundwater regimes are present: a deep aquifer (the most important in the UK in terms of annual yield) comprising Cretaceous chalk and the overlying Paleogene Thanet Formation; and the near-surface River Terrace Gravels. These two aquifers are separated by the Eocene-aged London clay, an effective aquitard, which rises up to form a range of hills 3 km W of Staines and completely isolates both aquifers hydraulically. While there exists an extensive literature on the hydrogeology of the Chalk (in particular, fracture-dominated primary transmissivity: e.g. Bloomfield, 1996), much less is known about that of the gravels, even though they dominate much sub-surface construction across the Thames

Basin. While both challenges (e.g. need for complex dewatering procedures during tunneling: Linde-Arias et al., 2018) and opportunities (e.g. exploiting gravel groundwater for refrigerant purposes: Birks et al., 2013) have been extensively described, these are generally couched in terms of their geotechnical aspects instead asking more fundamental questions of, for instance, flow rates, typical hydraulic conductivity values, or degree of heterogeneity.

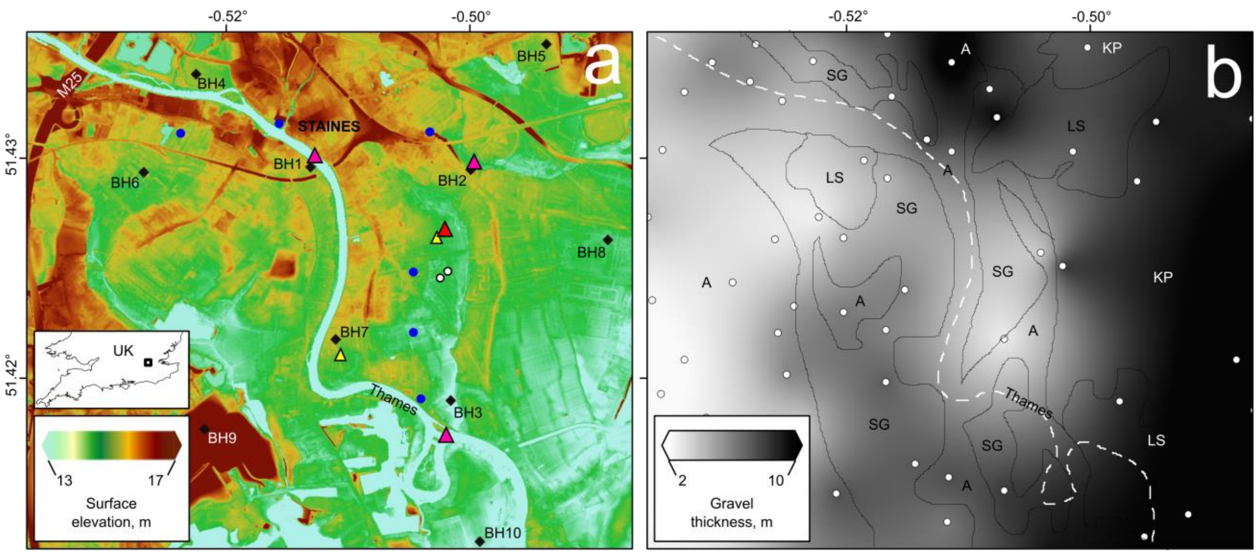

Figure 1. (**a**) Digital terrain model (DTM) of the Staines area, SE UK, from 1 m resolution lidar dataset (inset = location in southern UK). Red and pink triangles = river level gauges, and groundwater level and rain gauges respectively (location metadata in Table A1). Black diamonds = boreholes from which gravel samples were taken for laboratory analyses of hydraulic conductivity and flow rates (Table A2). Blue circles = groundwater sampling points for hydrochemical analyses (Table 2; Table A3). White circles = twin tube wells where pumping test was conducted (Table A3). Yellow triangles = location of seismic refraction surveys, used to validate GPR spot measurements of groundwater level (Table A1). (**b**) Thickness of river terrace gravels and alluvium. White circles = position of borehole stratigraphic logs (Table A4). A = alluvium; LS = Langley Silt Member; SG = Shepperton Gravel Member; KP = Kempton Park Gravel Member. White dashed line = course of River Thames.

The River Terrace Gravels, hereafter considered a single unit, were deposited on a broad river plain during colder periods of the Pleistocene. These gravels, typically undifferentiated in borehole logs, vary in thickness in the Staines region, generally thinning to the N and W, but with important local variations (Figure 1b). Significant demand for aggregates since the 1940s in the UK has led to the extensive exploitation of the gravels, with old worked-out pits typically lined and backfilled with waste materials, which has a profound hydrogeological impact by local raising or lowering groundwater levels, leading to discrete patches of groundwater emergence and surface water pollution (Morgan-Jones et al., 1984).

Elsewhere, laboratory flow experiments using River Terrace Gravels (within a suite of different aggregates) demonstrated that linear (i.e. Darcyan) flow breaks down as the gravels became coarser, becoming more similar to turbulent flow in rough-walled pipes. This was explained, and Darcy's Law could be applied, via considering a gradient dependence of hydraulic conductivity for gravels (Mulqueen, 2005).

1.3 Motivation and Objectives

We spoke to local residents across Staines as part of this project, many of whom commented on rising flood frequency over a 10–20-year period, in increasingly "unexpected" places i.e. basements far from rivers and other surface water, and not within the Environment Agency's highest-risk "Flood Zone 3b", i.e. >5% probability of flooding (EA, 2020). This risk classification, used by local and national government for major planning decisions, does not include groundwater flooding, which can significantly exacerbate or prolong fluvial flooding (Parkin, 2024).

The purpose of this study was therefore to investigate the magnitude and spatial distribution of groundwater flooding in an area characterized by highly permeable near-surface superficial deposits (River Terrace Gravels) that has been perturbed by extensive urbanization, groundwater abstraction, and gravel extraction. We focused our investigation over a short, intense period in early January 2024, where much of southern England (including the Staines region) experienced the most severe flooding since 2014 (Fan, 2024), with 68 mm of rain falling in a six-day period (December 31 2023 – January 5 2024; 12% of the annual mean of 585 mm for Staines), which raised river and groundwater levels by up to 2 m, causing extensive flooding.

We leveraged our existing local stakeholder contacts to design a participatory data collection program, following guidelines for citizen science approaches in hydrology (Section 2.1; e.g. Buytaert et al., 2014; Paul et al., 2018; Nardi et al., 2022). This allowed for a novel combination of sub-surface hydrologic and near-surface geophysical surveys and laboratory analyses, to address the following specific questions:

1. What is the disposition of the water table in the gravels at a single time following extreme rainfall (in early January 2024)?
2. What are typical flow rates through the gravels; do these rates depend on the type of test (laboratory or pumping) through which they were determined? Birks et al. (2013) noted, for instance, a discrepancy of two orders of magnitude for values of K determined in the field and laboratory.
3. Does groundwater flow follow a simple regional head gradient, or are local variations (e.g. obstacles such as clay-lined backfilled gravel pits), or the heterogeneity of the gravels themselves, significant?
4. Is surface topography, moderated by urbanization, the primary control on the spatial distribution of groundwater flooding, as suggested for the city of Oxford (60 km NW of Staines, also on the River Thames and a similar floodplain gravel substrate) by Macdonald et al. (2012)?
5. To what extent is observed flooding groundwater-related, since patches of surface and basement flooding are reported far from any surface drainage.
6. Which observations should be included to develop a groundwater emergence risk map, beyond the comparatively sparse and low-spatial-resolution topographic and hydrogeologic datasets employed at a regional scale (e.g. McKenzie et al., 2012; Defra, 2020)?

2 Materials and Methods

We employed an approach that catalyzed the involvement of local stakeholders (Section 2.1) to inform the location of geophysical and hydrologic field techniques (Sections 2.2 and 2.4, respectively). Groundwater flow simulations are detailed in Section 2.3, while laboratory analyses of aquifer rock and groundwater are discussed in Section 2.5.

2.1 Community Mobilization

We sought to leverage local knowledge on historical flood duration, locations, and magnitudes, in order to inform our data collection strategy. First, we identified a local community champion (or “social mobiliser” – e.g. Buytaert et al., 2014), who organized two townhall-style meetings in

November 2023 and January 2024 that were attended by ~50 local residents, business owners, and representatives of local government. These stakeholders reported a desire to gain some agency over their immediate (hydrologic) environment, i.e. gaining an understanding of flood risk and prevention.

In January 2024, participants plotted areas of residential or street flooding on a local map, as well as other hydrologic features of interest including buildings with deep basements, backfilled gravel pits, and groundwater abstraction locations (Table A3). These locations were independently verified following the stakeholder meeting via site visits, and consultation with the local Council planning registry, 19th Century six-inch Ordnance Survey maps, and the British Geological Survey GeoIndex borehole database, respectively. The meeting yielded candidate localities for seismic refraction surveys (Section 2.2), which required open access and permission to operate across farmland or fields, as well as potential localities where observation wells might be bored for the purpose of gravel sampling and groundwater level monitoring.

Residents were also invited to participate in the geophysical surveys, while the location of a pumping test (Section 2.4) was suggested in an allotment where twin 5 m tube wells had recently been installed. Flood locations (N = 65 – Table A3 – via email to the community champion) were relayed for two weeks following the January 2024 meeting.

2.2 Geophysical Surveys

Ground-penetrating radar (GPR), typically used for near-surface geotechnical and civil engineering applications e.g. pipe and void detection, has recently been exploited in hydrologic investigations both in boreholes (e.g. Gueting et al., 2017) and at the surface. Doolittle et al. (2006) described how a series of “spot measurements” (5–20 m-long local transects) might be stitched together to reveal spatial variations in water table depths. If these snapshots were repeated, local groundwater flow patterns might be elucidated. Here, we captured >140 short GPR transects (Table A5) across a ~20 km^2 area of southern Staines, suggested by local stakeholders to experience intense, yet localized, annual (groundwater) flooding. Surveys were conducted on 7 and 14 January at identical locations. The network of GPR sampling points was dictated by access so necessarily follows major roads and pathways to enhance fair spatial coverage across the region. The radar unit used was a Radiodetection LMX200 with a 250 MHz antenna. The LMX200 consists of a digital control unit with a keypad, VGA video screen, and connector panel. A 12 V battery powered the system, which was pushed across each 10–20 m transect on a four-wheeled dolly. For depth conversion we assumed a radar velocity of 0.12 ns m^{-1}, which falls within the range of reported GPR velocities for "dry gravel" (0.10–0.16 ns m^{-1}) and "wet gravel" (0.06–0.13 ns m^{-1}; Tillard and Dubois, 1995).

In order to benchmark these GPR estimates, we (a) conducted two 10 kg sledgehammer-shot seismic refraction surveys (Table A1), such that the sub-surface velocity structure might be sought, and (b) took contemporaneous dip meter readings at 10 wells (Table A2; Section 2.4). 48 shot records were collected using a Geometrics 24-channel seismograph and 10-hit vertical stacking. We used 24 40 Hz Schlumberger geophones on 14 cm spikes, which were equally spaced at 1 m, with an off-end geometry setup. The chosen sample interval was 0.25 ms with a delay time of 10 ms; the record length was 250 ms, appropriate for shallow (<20 m) imaging (e.g. Keiswetter and Steeple, 1994). Stacking took place automatically following each succession of hits to ensure good source-ground coupling.

We used the SeisImager plotrefa routine (Geometrics and OYO, 2009) for time-term (i.e. simple travel-time) inversion, for its computational stability and sensitivity to small-scale (~m) structure changes (van der Veen et al., 2000). This relatively simple, lower-budget technique combines delay-time analysis and linear least-squares to invert first-arrivals for a velocity section. . The inverse velocity model was chosen as that with a matrix inversion error of <1.5% that balanced model smoothness with RMS misfit.

2.3 Groundwater flow modeling

We used two initial head distributions to estimate groundwater flow direction and level following a single one-week stress period in Modflow 6, coupled to the ModelMuse interface. The first distribution is the only available independent estimate of regional groundwater levels (South West Suburban Water Company, 1971; Sumbler, 1996); the second, our estimates of head on January 7 2024, using GPR (Section 2.2). We used a structured grid of 23 x 25 200 m resolution pixels as a compromise between computational expense and spatial resolution, and the RIV (River Package) to model the behavior of the River Thames. No-flow boundaries were imposed around pixels representing the position of basements and impermeable-lined backfilled gravel pits that extend through the entire thickness of the aquifer. Model parameters are detailed in Table 1.

Table 1. Groundwater flow simulation parameters. † = Mavroulidou et al. (1998); ‡ = Allen et al. (1997); ⁂ = Sumbler (1996). All other figures = this study.

Layer	k_H (ms^{-1})	k_V (ms^{-1})	S_s (m^{-1})	S_y (-)	ϕ (-)	Top (mAOD)	Base (mAOD)	Conductance (m^2s^{-1})	Stage (m)
1 – River Terrace Gravels	0.01	0.01	4 x 10^{-4} ‡	0.25 ‡	0.30	Surface topography (i.e. free surface)	Per calculations in Fig. 1b	-	-
2 – London clay	1.16 x 10^{-9} †	1.16 x 10^{-10} †	10^{-4} †	0.02 †	0.45 ‡	Base layer 1 (per Fig. 1b)	0	-	-
(River Thames)	-	-	-	-	-	Per lidar DTM (Fig. 1a)	-	10^{-6} ⁂	Per gauging stations (Fig. 1a)

2.4 Hydrologic Surveys

We bored 10 observation wells at spatially representative locations across Staines where local permissions and continued access could be rapidly guaranteed (Table A2). These were simply constructed, using 4–5 m lengths of 3” (76 mm) sharpened galvanized steel scaffolding that were inserted into the ground using a percussive hammer. Each well was lined with 76 mm diameter schedule 40 PVC piping, into which 50 mm-spaced 10 mm diameter slots were cut on opposite sides of the pipe. Each well was covered with geofabric to restrict the ingress of soil particles. Each well was open to the gravel aquifer; measurements of groundwater level were taken on 7 and 14 January 2024 using an SCCS 15 m electronic water level gauge dip-meter, which was powered by a 9 V battery. Gravel was initially removed from each well for flow rate laboratory testing (Section 2.5).

We also installed a co-located rain gauge and automatic groundwater level monitor in November 2023 (Table A1). These were placed in the garden of a local resident to minimize the risk of theft. We used a 0.2 mm Davis automatic tipping-bucket rain collector that was connected to an Onset HOBO Pendant datalogger, recording rainfall at 15-minute intervals. The groundwater monitor was a Solinist Levelogger 5, which used a Hastelloy pressure sensor (accurate to ±0.8 mm) to record water table level at 15-minute intervals. River level data were sourced from Environment Agency ultrasonic gauges at two points on the River Thames and one at the smaller

River Ash (Table A1; Figure 1a).

Tracer tests were conducted on 7 January 2024 using a single injection borehole and 17 monitoring boreholes (Table A6) guided by balancing even spatial coverage with access limitations. We used fluorescein dye due to its low sorptivity, capability to be visualized at low concentrations, and relatively short half-life of ~6 hr (due to high rates of photodegradation: Feuerstein and Selleck, 1963). Following the technique outlined by Kasanavia et al. (1999), we injected a 1 L slug of 100,000 mg L^{-1} concentrated fluorescein solution at 2 m depth in the injection borehole, using a large syringe. At each monitoring borehole we inserted an Aquaprobe AP-Lite GPS Aquameter, connected to a fluorescein optical electrode, at 2 m depth. This is a low-power instrument that detects fluorescein breakthrough using modulated yellow-green LEDs and a narrow-band excitation filter; it is connected to a field laptop that records dye concentration (initially as an output voltage proportional to concentration) at 1 s intervals. We matched the time to the breakthrough data peak with an ADE solution for instantaneous slug injection to obtain best-fit estimates of tracer transit time t, by minimizing the sum of squared errors between the observed data and the ADE solution.

To validate the experimental results (Section 2.5) of aquifer properties (i.e. transmissivity and hydraulic conductivity), we conducted a constant rate pumping test over eight days in January 2024 by exploiting twin 5 m, 2” (51 mm) bore tube wells, sited ~25 m apart, in a local allotment (Table A3). We used a Pedrollo DAVIS borehole pump with peripheral impeller to achieve a constant pumping rate of 15 L s^{-1}. In the observation well, we sought to balance between capturing the drawdown and recovery curve, and making excessive measurements/site visits, by adjusting measurement frequency, from every 30 mins in the first two hours, to every day after two days. We used a 15 m SCCS electronic water level dipmeter connected to a 9 V battery. To interpret the data, we used the AQTESOLV software (Duffield, 2007), which matches the Theis (1935)-type curve to drawdown data in logarithmic space.

The analysis of both drawdown and recovery data together exploits the application of superposition in time (e.g. Agarwal, 1980).

2.5 Laboratory Testing

We passed the borehole-collected gravel samples (Section 2.4) through a 4.75 mm sieve (U.S. standard 4; black), followed by a 2 mm sieve (U.S. standard 10; grey), which accounted for

100% of the samples taken. An experimental rig was constructed (Figure 2) to investigate hydraulic conductivity K as a function of hydraulic gradient (Mulqueen, 2005). This arrangement consisted of a 10 m-long, 76 mm diameter PVC pipe with retainer screens at both ends, which was packed with respectively 2 mm and 4.75 mm gravel, and connected to a 10 m^3 sump reservoir placed on a vertically adjustable support. Hydraulic gradient was systematically varied from 0.01–0.10 and flow rates measured. Water drained from the gravel-packed pipe into a graduated bucket. Least-squares regression was used to calculate best-fitting relationships between flow rates and hydraulic gradient for each grade of gravel.

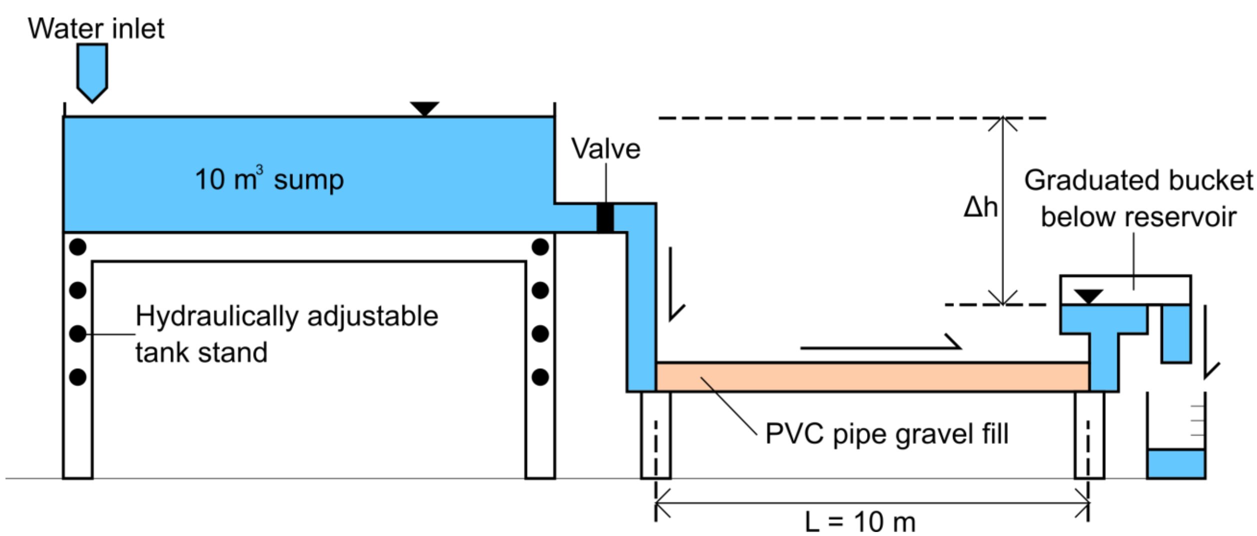

Figure 2. Experimental setup for measuring K and flow through river terrace gravels

Water samples were collected, in 200 mL rinsed polyethylene flasks, on 7 January 2024 from the River Thames under Staines Bridge, a small tube well in a local resident's garden that was bored into the gravel aquifer, and from four basements that were flooded to a depth of >30 cm (Table A3). From the tube well, the initial 10–15 min of pumped groundwater was discarded to ensure that the groundwater samples were representative of that in the aquifer. Two samples were taken at each locality, respectively for cation and anion analysis; they were filtered immediately using a 0.45 μm MF-millipore membrane, then stored in 60 mL HDPE bottles. Br^-, Fl^-, Cl^-, CO_3^{2-}, and HCO_3^- were determined in the laboratory by volumetric titration; SO_4^{2-}, PO_4^{2-} and NO_3^- concentrations were determined with a UV-VIS spectrophotometer. Cation (i.e. NH_4^+, Na^+, Ca^{2+}, Mg^{2+}, K^+) concentrations were determined by inductively coupled plasma-mass spectrometry

(ICP-MS) following the US Environmental Protection Agency (EPA) standard methods (Baird and Bridgewater, 2017). The laboratory values were compared to WHO (2011) potable water "safe" standards. Piper diagrams were then constructed using these data, in order to determine the provenance of the flood water.

3 Results

Figure 3 is a radargram, i.e. an example of raw GPR data, complete with artefacts including ringing and diffractions from sub-surface infrastructure. This section displays a clear reflector at ~18 ns time (~2.2 m depth). Also shown is a co-located spot well measurement of groundwater level (2.16 m depth), and the best-fitting sub-surface velocity model that was derived from inverting seismic refraction data. This model divided the sub-surface into three layers in which V_p = 1.1, 1.2, and 1.7 km s^{-1}, which correspond to sonic velocities of dry and wet gravel (~0.5–1.2 and ~1.5–2.0 respectively: Sharma, 1997; Bery and Saad, 2012; Xayavong et al., 2020).

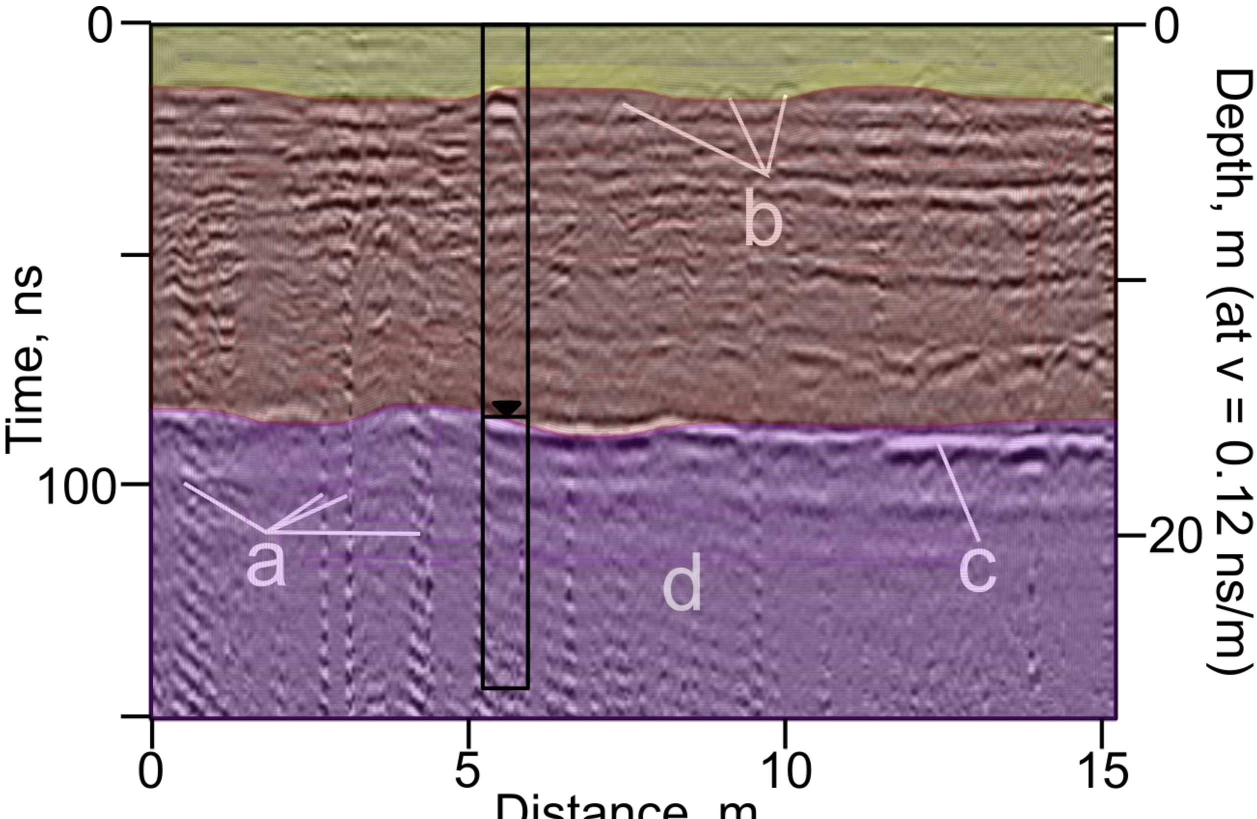

Figure 3. GPR radargram example (locality ID = GPR47 in Table A5; surface elevation = 16.90 mAOD; mean (interpreted) water table level = 14.70 mAOD). Shown are (a) ringing from

proximal infrastructure; (b) diffractions from near-surface buried pipes and cables; (c) reflected signal corresponding to water table. Groundwater level was measured in BH7 (Table A2) using an electronic dip-meter as 14.74 mAOD, shown above as 2.16 m below surface level. Colours = best-fitting P-wave velocity model from seismic refraction data. Yellow = 1.1 km s^{-1}; pink = 1.2 km s^{-1}; purple = 1.7 km s^{-1}.

Figure 4 contains maps of hydraulic head and depth to groundwater for a region of Staines on January 7 and 14, 2024. This surface was generated using all GPR spot estimates, together with contemporaneous well measurements. Figure 4 also shows contours of tracer transit time (in hours) from the injection well to peak breakthrough recorded at each of the measurement boreholes.

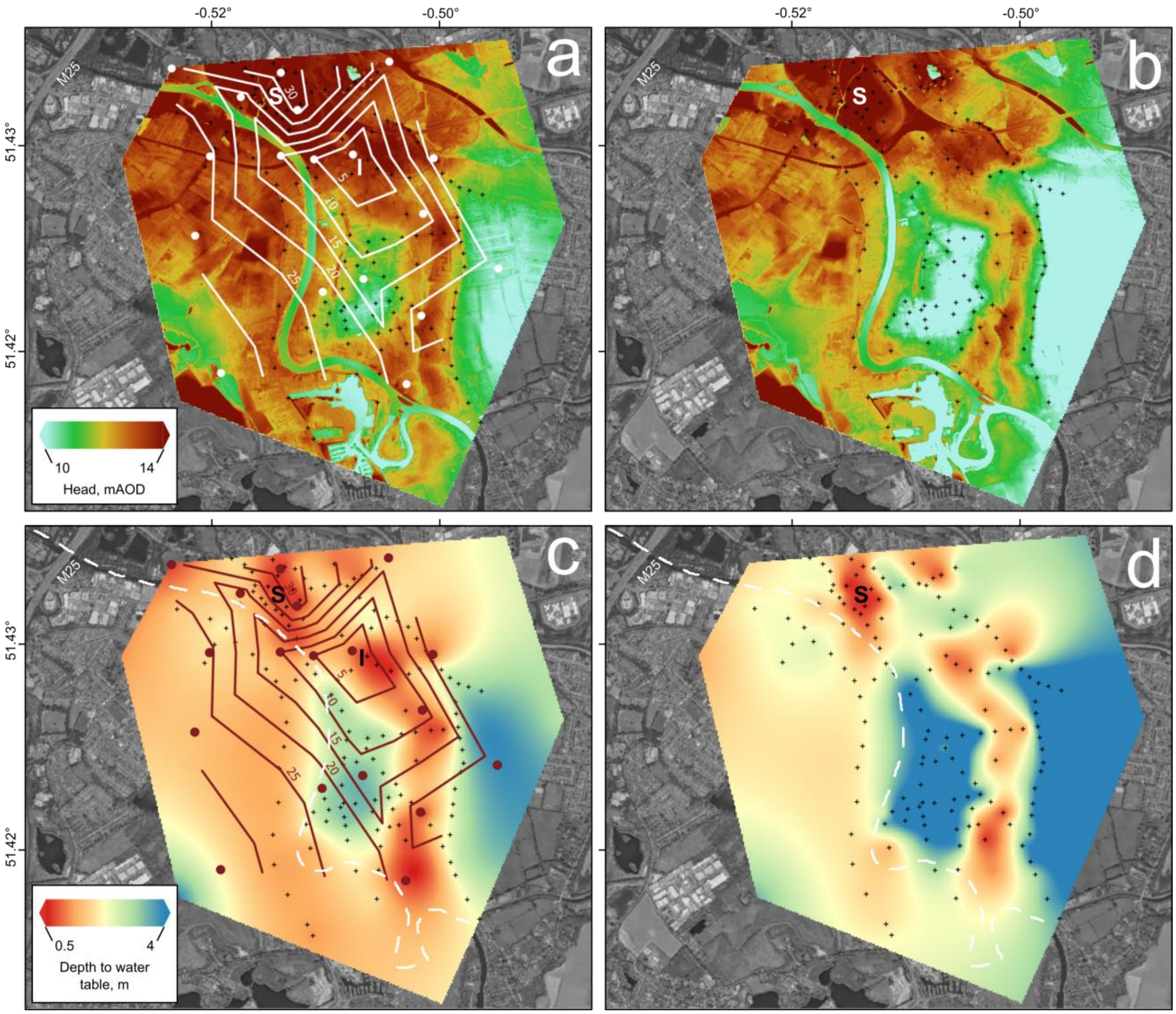

Figure 4. Hydraulic head and depth to groundwater on respectively (**a** and **c**) January 7 and (**b** and **d**) January 14 2024. Black crosses = locations of GPR spot measurement. S = Staines town center. White dashed line = trace of River Thames. Background = Google Earth Satellite imagery. Circles and contours on (**a** and **c**): boreholes where tracer concentration was measured on January 7 2024, and tracer travel time (in hours), respectively. I = injector well. GPR and tracer borehole localities are presented Tables A5 and A6 respectively.

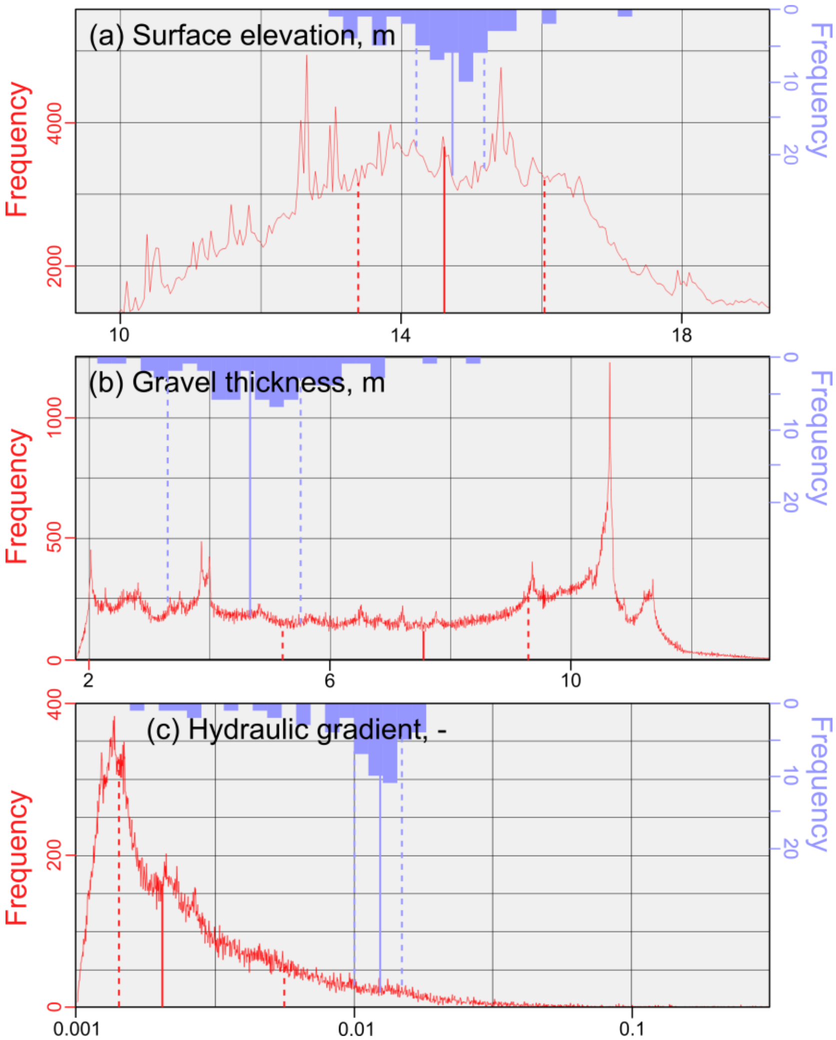

Figure 5. Histograms of incidents of reported groundwater flooding (blue; N = 65; see Table A3 for locations) against local (**a**) surface elevation from high-resolution (1 m) lidar DTM dataset; (**b**) river terrace/alluvium gravel thickness; and (**c**) hydraulic gradient (averaged across a 100 m kernel). Thick and dashed vertical lines = mean value and one standard deviation, respectively.

Figure 5 presents three histograms that compare the distribution of flooding locations, recorded by residents and verified over January 7–14 2024 (Table A3; N = 65), with (a) local surface elevation (Figure 1a), (b) local aquifer thickness (Figure 1b), and (c) local hydraulic gradient, averaged over a 100 m kernel from each flooding locality, across the Staines region. Using the AQTESOLV software, the best-fitting Theis (1935)-type curve yielded the following values: storativity = 0.026, transmissivity = 2585 m^2d^{-1}. An estimate of hydraulic conductivity = 873 md^{-1} (0.010 ms^{-1}) was obtained by considering the saturated zone thickness of 2.96 m. A pumping test by the South West Suburban Water Company (1971), at a nearby location (350 m from the present test) recorded a similar value of hydraulic conductivity = 1170 md^{-1} (0.014 ms^{-1}) for the River Terrace Gravels, together with a storativity of 0.06 and transmissivity of 1620 m^2d^{-1}.

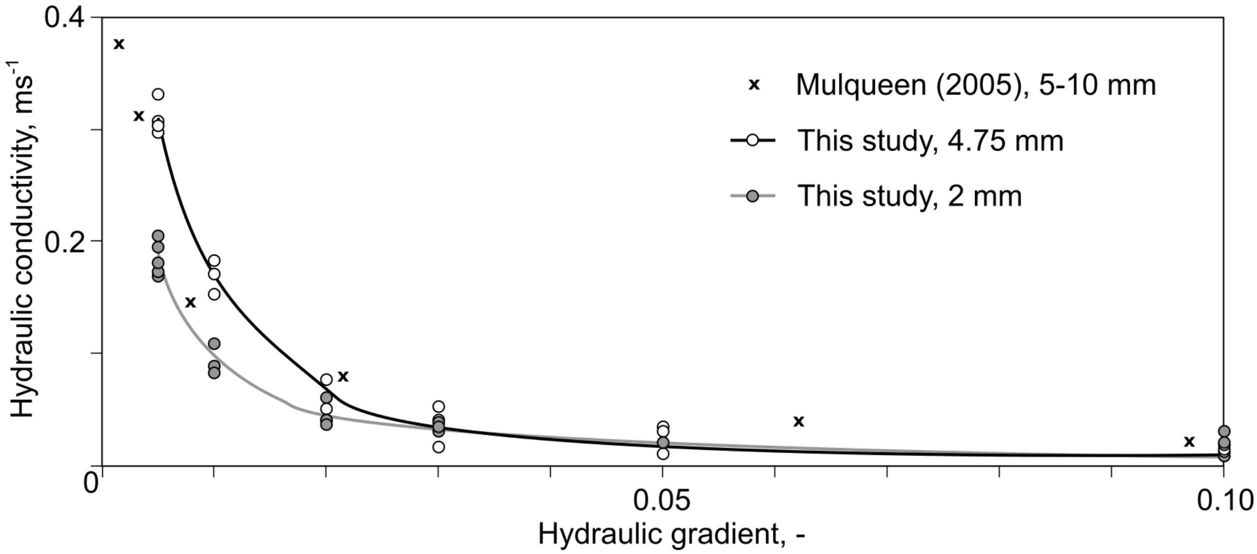

Figure 6. Measured hydraulic conductivity K as a function of hydraulic gradient, dh/dL, for river terrace gravels obtained from 10 boreholes (Fig. 1a; see Table A2 for locations). 100% of the gravel samples either passed through a 4.75 mm sieve (U.S. standard 4; black) or 2 mm sieve (U.S. standard 10; grey).

Figure 6 shows hydraulic conductivity K, measured in the laboratory for two sampled gravel grades (Figure 2), as a function of hydraulic gradient dh/dL, together with data from Mulqueen (2005). A non-linear relationship is observed between flow velocity and hydraulic gradient, suggesting that Darcy's Law does not hold for groundwater flow through these gravels. Least-squares regression yielded the following best-fit relationships for 4.75 mm and 2 mm grade gravel respectively: $K = 5100(dh/dL)^{-0.35}$ and $K = 1350(dh/dL)^{-0.18}$. For 5–10 mm grade gravels, Mulqueen (2005) reported the relationship $K = 1918(dh/dL)^{-0.13}$.

Table 2. Analytical results of water quality for samples pumped from gravel aquifer (N = 2), and taken from basement flood water (N = 4) and River Thames (N = 6). Sampling locations are given in Table A3.

Mean ion	**Na^+**	**NH_4^+**	**Ca^{2+}**	**Mg^{2+}**	**K^+**	**Cl^-**	**Br^-**	**NO_3^-**	**PO_4^{2-}**	**HCO_3^-**	**CO_3^{2-}**	**Fl^-**	**SO_4^{2-}**

content (mg L^{-1})													
Pumped groundwater (N = 2)	35.25	0.017	101.68	4.76	6.63	43.72	0.058	25.71	0.84	24	370	0.11	55.96
Flood water (N = 4)	36.10	0.012	103.45	4.78	6.49	42.96	0.055	25.43	0.84	28	336	0.11	58.34
River Thames water (N = 6)	24.72	0.046	108.53	4.44	4.47	35.87	0.051	26.87	0.16	245	232	0.10	38.78
WHO (2011) drinking water standards	200	0.2	75	30	100	200	0.5	50	40	200	500	1.5	200

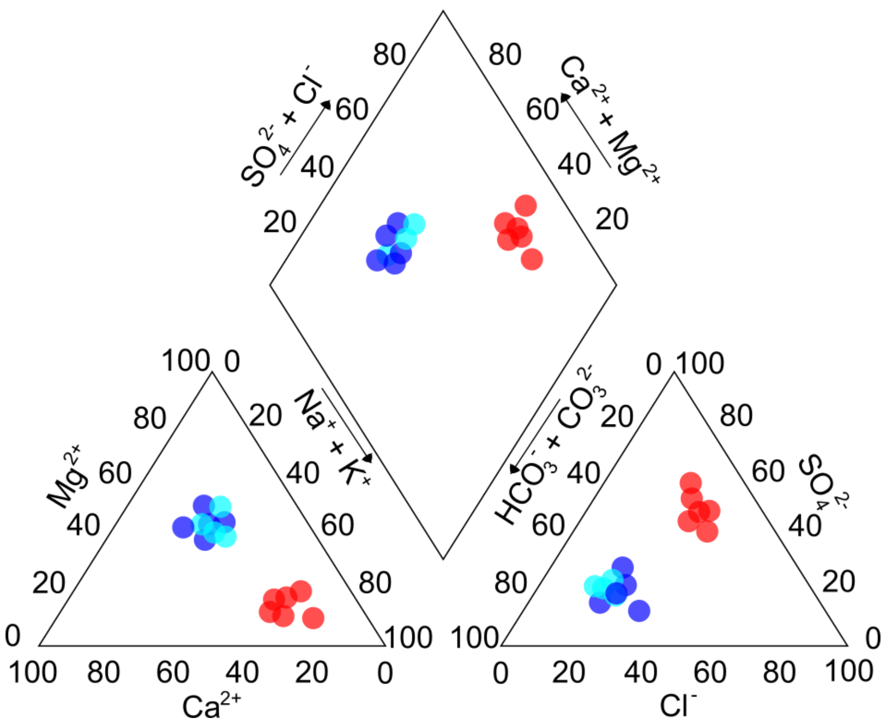

Figure 7. Piper diagram of hydrochemistry (Table 2) of River Thames water (red), pumped groundwater from gravel aquifer (light blue), and flood water (dark blue).

Figure 7 is a Piper diagram that shows the composition of water sampled from the River Thames, the gravel aquifer, and locations of basement flooding (Table A3). Major and trace cation and anion concentrations are reported in Table 2. The results indicate that the river water may be uniformly characterized as SO_4.Na-Cl type, while the groundwater and floodwater, while chemically distinct from the river water, may together be weakly characterized as HCO_3-Mg.

4 Discussion

4.1 Groundwater Level Variation

The GPR technique worked well as a means to estimate groundwater level non-invasively over a wide (~20 km^2) area in a single day. Accuracy was <±15 cm of each nearby observation well in all cases, which agrees with the findings of Essam et al. (2020), who were able to determine groundwater levels using GPR to within <±25 cm in 40 localities. The results of inverting two sets of seismic refraction data yielded simple three-layer velocity models, where the largest increase in velocity (from 1.2 to 1.7 km s^{-1}) corresponded to a locally important (in the absence of significant changes in stratigraphy in the top 10 m below surface) increase in acoustic impedance, at the water table. Van Overmeeren et al. (2004) suggested caution be taken when using GPR for hydropedologic purposes due to thick capillary zones in many soils; however, this was not observed in the relatively coarse River Terrace Gravels (grain size typically 1–5 mm). Figure 5 demonstrates dramatic hydraulic gradients over relatively short distances (to a maximum of ~1 m over ~100 m) in the Staines region on two dates in early January 2024. This contrasts against the modest and uniform NW-SE regional gradient observed, on the basis of dipping six wells, in July 1970 by South West Suburban Water Company (1971). This section considers possible explanations for these local variations.

Larkin and Sharp (1992) note that in many urban floodplains with negligible variations in surface topography, underflow, baseflow, and influent/effluent river-groundwater fluxes interact with sub-surface infrastructure in a manner that generates large head variations over short distances. The disconnect between River Thames stage and groundwater level, however, was unexpected: the former responding over a timescale of ~days to extreme rainfall events in end-November and end-December 2023; the latter, over ~weeks (Figure 8). Moreover, variations in head are spatially independent of the river (Figure 4), while flood water, even from properties and locations adjacent to the River Thames, is clearly of a chemical affinity resembling pumped groundwater (Figure 7). These findings stand in opposition to those of Wilson (1984) and Kim et al. (2016), who suggested that river stage held the strongest influence on groundwater level in urban areas near major rivers. In the Staines area, the hyporheic zone is known to be particularly thick (>10 m: Ellison et al., 2004), while the River Thames has not been dredged since the late 1950s (Sumbler, 1996). Theoretical studies have suggested the dominant controls of seasonal groundwater fluctuations on expanding the hyporheic zone, hindering water movement and biogeochemical cycling (Wondzell and Swanson, 1999; Malzone et al., 2016).

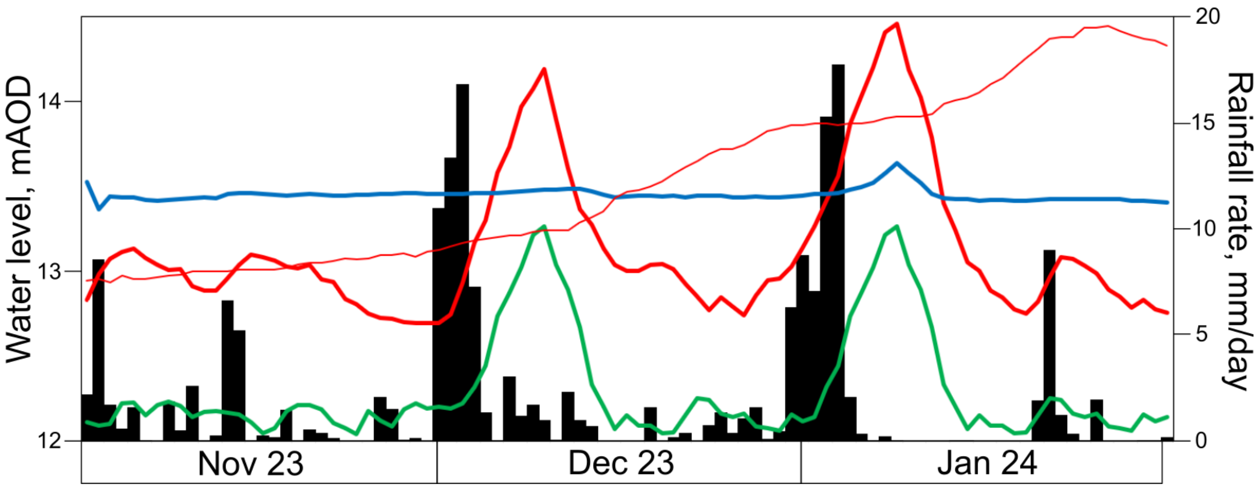

Figure 8. Rainfall, groundwater and river levels for Staines, November 2023 – January 2024. See Fig. 1a for location of gauging stations. Black bars = daily rainfall rate; thin red line = groundwater level; thick colored lines = river levels (red = R. Thames upstream, Staines town center; green = R. Thames downstream, Penton Hook Lock; blue = R. Ash).

Figure 4 also shows a raising of head close to Staines town center, which could result from multiple deep excavations in the area (for new building projects) for acting as drains. In this case, the new free surfaces generated alter the local stress state such that water is drawn to intersect the surface at 90° (e.g. Ding et al., 2008). Elsewhere, groundwater level is 1–2 m higher below the west bank (relative to the east) of the River Thames, which acts as a local government boundary. The authority covering the west bank (Runnymede Borough Council) installed soakaway drainage over its entire road system in the early 2010s. Soakaways have been shown to induce rising groundwater levels, groundwater mounds, and highly localized surface flooding that can create potential risks for residential (basement) flooding (e.g. Roldin et al., 2013). These effects have been extensively modeled and described in the literature; the general conclusion is that such infiltration-based stormwater systems can lead to an important and sustained increase in local groundwater levels, which is especially pronounced in systems composed of high-permeability superficial deposits (Maimone et al., 2011; Roldin et al., 2013).

4.2 Groundwater Flow

Laboratory testing revealed non-Darcyan flow through the gravels at low hydraulic gradients, with hydraulic conductivity K a non-linear function of gradient, similar to that observed elsewhere for other gravels and aggregates (Figure 6; Mulqueen, 2005). Large hydraulic gradients (>0.05) yield linear flow regimes and lower-bound estimates for K ≈ 0.01–0.04 ms^{-1}, which agree with values derived from pumping tests (K = 0.010 ms^{-1}), both as part of this study in January 2024 and from a nearby 1970 aquifer test experiment (0.014 ms^{-1}: South West Suburban Water Company, 1971).

At low gradients (< ~0.03), however, Darcyan flow behavior breaks down (Figure 6). Interestingly, the results from a single tracer test (with multiple observation wells: Figure 4a) reveals the presence of several faster-flow pathways through the gravels, notably towards the S and NW (with the latter aligning with the course of the River Thames, i.e. underflow). This behavior is more commonly expected in the underlying Chalk, where uneven dissolution – especially along valley bottoms and zones of water table fluctuation – tends to enlarge fractures and enhance primary transmissivity, even generating localized zones of karst (Bloomfield, 1996).

It is clear from Figure 4 that the River Terrace Gravels represent an aquifer in which groundwater flow is highly sensitive to the imposition of sub-surface obstacles such as deep basements and clay-lined backfilled gravel pits (Figure 9). Highly localized ironstone concretions are locally present, but are difficult to map owing to their swarm-like concentrated spatial pattern and limited extent (typically in 10–30 cm thick and <2 m long patches: Ellison et al., 2004).

The behavior of gravels and highly permeable (i.e. 10–10^5 D) unconsolidated sands has been extensively investigated from the perspective of petroleum engineering; in this case, pressure rather than elevation heads are more commonly discussed. Welch et al. (2014) consider small-scale (cm) lithological heterogeneity to control groundwater propagation in three Australian gravel aquifer systems. Alexander et al. (2011) note that ~4 x 10^5 measurements of K would be required to model deterministically tracer transport across an entire alluvial aquiver, in which K was observed to vary by over three orders of magnitude. They also note the scale effect, i.e. gravel aquifers may contain highly conductive zones that may not be “seen” by methods that sample spatially smaller volumes.

At the pore scale, the high porosity (~0.5) of the River Terrace Gravels and lack of cementation between the grains (Sumbler, 1996) implies they are close to the isostatic limit. This kind of system has been studied by numerous workers investigating water injection into poorly consolidated sand and gravel deposits: fluid pressure fluctuations are seen to interact with the contact stresses between grains, causing rearrangements in the grains that locally alter permeability and porosity (Ameen and Dahi Talghani, 2015). This effect can lead to matrix deformation that is completely different from that expected into hard rocks that are more prone to brittle failure, an effect especially true with low confining stresses (Gan et al., 2020). This is expected in the Staines region due to the shallow aquifer depths (generally <10 m below surface level to base gravel). Therefore, modest pressure or elevation heads would lead to highly non-Darcyan flow; indeed, channelization in gravel aquifers (resulting from internal erosion) has been extensively observed in other areas (Ameen and Dahi Talghani, 2015; Konstantinou and Biscontin, 2022). In this case, the observed preferential flow pathways are potentially generated when water-induced stresses become locally larger than a critical threshold, dislodging and carrying away smaller grains, leading to the (highly localized) evolution of porosity and permeability along the induced flow paths.

4.3 Groundwater Flooding and Risk Maps Revisited

Figure 9 shows 65 flooding localities identified by local stakeholders in January 2024. These were independently verified, while sub-sampling of the water suggests that groundwater emergence was the cause (rather than e.g. leaking mains water pipes, or river water: Figure 7). Although the participatory approaches were successful judging by the degree of engagement and volunteered geographic information (e.g. Nardi et al., 2022), it is likely that the true flood extent was not fully captured. However, it is apparent that the flooding was distributed in a pattern of small patches that was independent of the course of the River Thames. Flooding was not observed close to old, backfilled, clay-lined gravel pits, nor close to buildings with deep basements in the town center, suggesting that these local obstacles might divert groundwater flow elsewhere. Indeed, Ding et al. (2008) demonstrated how clusters of deep foundations effectively modify local aquifer hydraulic conductivity, acting as a barrier to hydraulic movement. Especially in shallow and thin aquifers (such as the River Terrace Gravels), the raising of groundwater levels on the “leeward” side of deep basements (in the presence of a regional hydraulic gradient) can be dramatic – by over 14 m, for instance, in some parts of Kong Kong, causing localized groundwater flooding (Jiao et al., 2006).

Figure 5 shows that the distribution of observed groundwater flooding does not correlate especially well with surface elevation: most floods occur close to the mean elevation for the Staines region (14.65 mAOD). Macdonald et al. (2012) cites topographical variations as the main factor dictating changes in groundwater flood vulnerability in nearby Oxford; yet many of these variations are related to urbanization e.g. sections of deep sheet piling, or the isolation of low-lying areas of floodplain as a result of surrounding constructions. Groundwater emergence is favored where the River Terrace Gravels are thinner (below the regional mean of ~7.5 m), for instance around regions where they might have been extracted in the 19^{th} Century (Morgan-Jones et al., 1984). However, the most striking observation is that groundwater flooding is concentrated in areas of high hydraulic gradient (>0.01, relative to a regional average of 0.003: Figure 5c). Robins and Finch (2012) note the positive correlation between volumes of groundwater emergence and the magnitude of “head differences” at several locations across southern England.

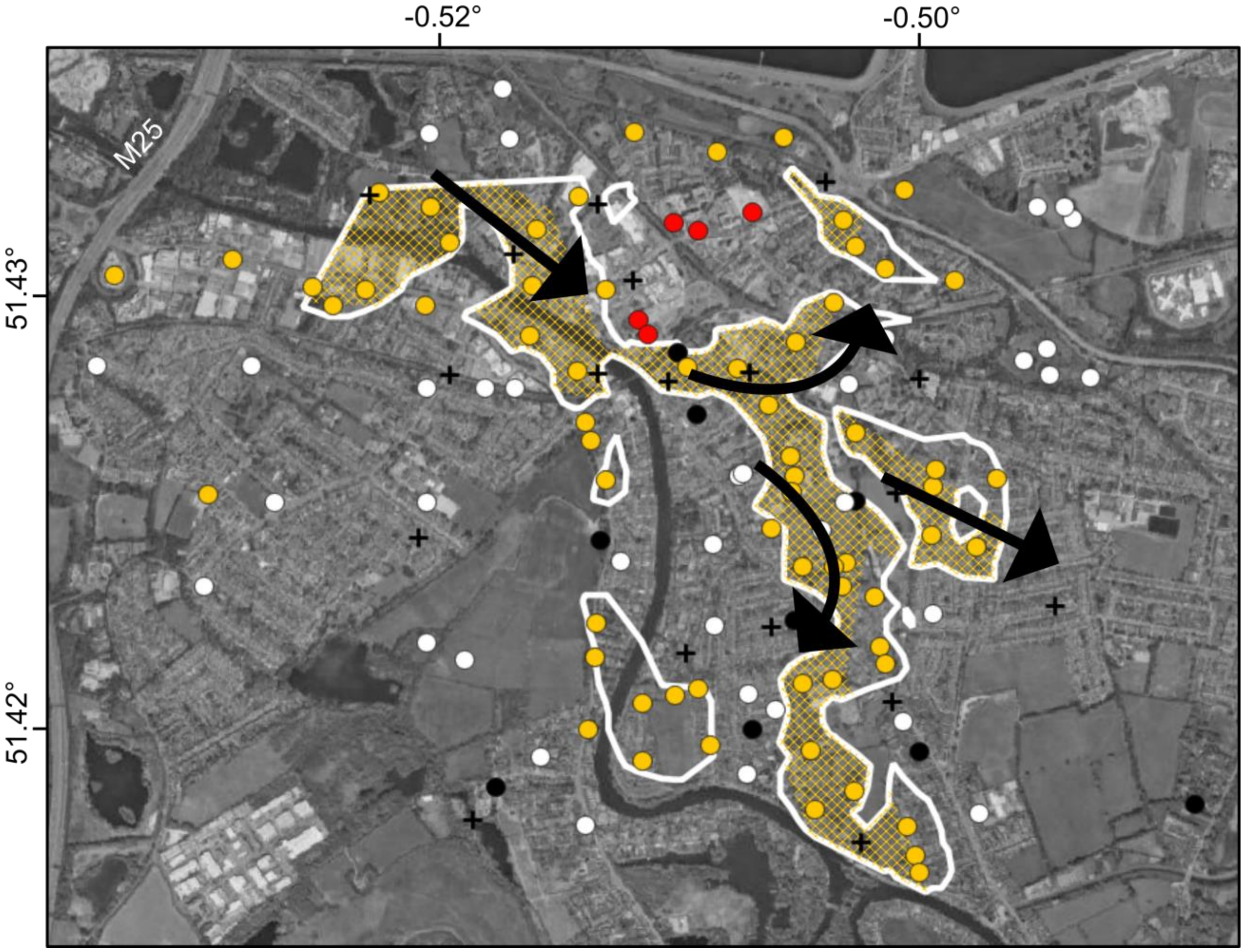

Figure 9. Groundwater flood risk map. Yellow circles = locations of groundwater flooding, initially reported by local residents, verified on January 2–10 2024. White circles = residential or industrial pumping sites from the gravel aquifer. Red circles = buildings whose basements extend through the gravel layer into the underlying London clay. Black circles = former gravel pits, now backfilled, picked from 1869, 1872, and 1897 six-inch Ordnance Survey maps. Metadata related to the positions of all the circles are detailed in Table A3. Crosses = tracer wells (Figure 4). White outline = zone where hydraulic gradient >0.01 on both January 7 and 14 2024, measured over 100 m grid squares. Yellow hatching indicates intersection of zones of high hydraulic gradient, fast (>0.01 ms^{-1}) groundwater flow pathways, and 95% of reported groundwater emergences. Black arrows = direction of flow in relation to hypothesized sub-surface barriers, based on tracer tests (Fig. 4).

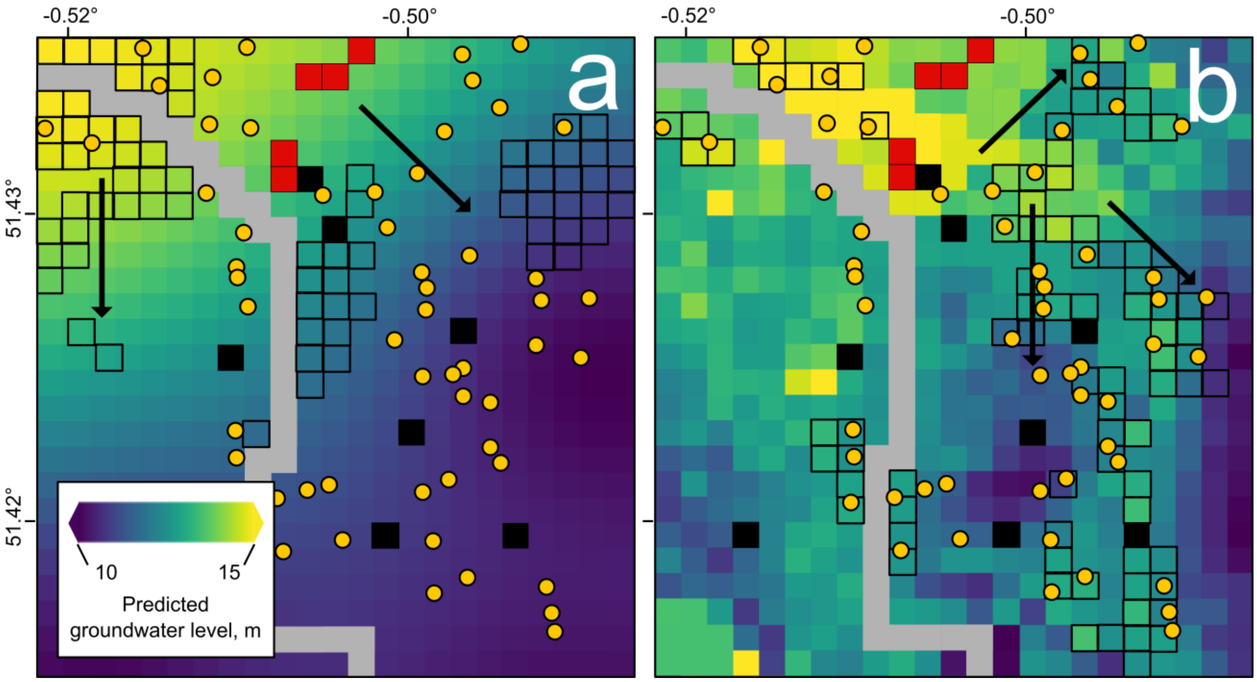

Figure 10. Simulated groundwater levels one week following initial head conditions: (a) estimate of simple regional ~NW-SE hydraulic gradient (South West Suburban Water Company, 1971); (b) situation on January 7, 2024 (Fig. 4a). Arrows = groundwater flow directions. Red and black squares = no-flow boundaries due to basements that extend through gravel aquifer, and impermeable-lined backfilled gravel pits, respectively. Gray squares = River Thames. Yellow circles = verified groundwater flooding locations (per Fig. 9). Black-outlined squares = regions where head > surface level (i.e. predicted groundwater emergence).

At the townhall-style stakeholder workshops, many residents expressed an urgent need to "stop" or "prevent" the recent floods, rather than solely characterize their origin and causes, as well as a frustration at the inability of existing regulatory structures to do so. While existing fluvial flood risk maps typically describe the risk of 10- or 100-year events based on the assembly of a sophisticated variety of datasets (e.g. topography, historical flood extents, river stage and flow time series), the construction of groundwater flood risk maps typically follows an ad hoc protocol, taking in more sparse and lower-resolution data of e.g. transmissivity, permeability, and groundwater level (Morris et al., 2007). Figure 9 presents a groundwater flood risk map for the Staines area that includes verified local observations of (groundwater) flooding, and zones of high hydraulic gradient (calculated from hydraulic head in January 2024). These datasets explore the novel approach pioneered by Defra (2020), who note the importance of including local and historical flood observations in such risk maps. Robins and Finch (2012) and Dochartaigh et al. (2019) note the correlation between patterns of observed groundwater flooding and high hydraulic heads, which are seen to "[m]aintain flooding for weeks, with important implications for infrastructure development".

Figure 10 shows predicted groundwater levels and flow directions in response to two initial head distributions. South West Suburban Water Company (1971) and Sumbler (1996) used sparse data to suggest a regional ~NW-SE head gradient, which translates to discrete patches of predicted groundwater emergence (i.e. head > surface elevation) in the north of the study area that do not match actual flooding locations in January 2024. On the other hand, the head distribution mapped by GPR on January 7, 2024 (Fig. 4b) yields S/SE groundwater flow vectors that agree well with the strike of fast-flow pathways suggested by tracer testing (Figs. 4 and 9). Moreover, taking into account the distribution of sub-surface obstacles (i.e. basements and gravel pits) that penetrate the entire aquifer thickness and obstruct flow, the predicted areas of groundwater emergence correlate remarkably well to verified flood locations, notwithstanding the relatively low (200 x 200 m) spatial footprint of the former. In this case, 43 of 54 (~80%) of actual flood locations map onto pixels where head is greater than surface level. Combined with the equally good spatial correlation between implied groundwater flood risk (Fig. 9) and predicted groundwater emergence areas (Fig. 10), our results suggest that aquifer thickness variations, moderated by sub-surface flow obstacles, generate localized head variations leading to fast groundwater flow pathways that explain the complex distribution of observed groundwater flooding.

Figure 10 also demonstrates that the River Thames does not exert an important influence on groundwater levels (cf. Fig. 8). Cores from the riverbed under Staines Bridge show that 3.6–3.8 m of fluvial muds lie directly on impermeable London clay, suggesting a much thicker hyporheic zone here than at Oxford or London (e.g. Sumbler, 1996). This agrees with local evidence of the Thames not having been dredged since 1968 (e.g. South West Suburban Water Company, 1971). Instead, relative changes in aquifer thickness and hydraulic gradient govern groundwater flow and emergence. These results and our approach are generalizable to a range of other urbanized catchments where gravels form an important superficial aquifer, such as Singapore, Los Angeles, London, and Sydney.

The principal challenge now will come from translating these exploratory, high spatial resolution

– yet localized – findings, into regulatory frameworks that (a) do not explicitly consider groundwater emergence in the construction of flood risk maps (EA, 2020; Parkin, 2024), and (b) are necessarily concerned with generalizing across much larger (national) scales, where hydrologic data are sparser and other observables (e.g. elevation models and stratigraphy) lower resolution.

5 Conclusions

We conducted a spatiotemporally intense investigation of groundwater flow and level variation in the River Terrace Gravel aquifer of southern UK in January 2024. A method was designed that leveraged and mobilized local knowledge and participation, and combined near-surface geophysics (GPR and seismic refraction surveys) with more traditional hydrogeological pumping and tracer tests, and laboratory analyses of flow rate and water chemistry. The following brief conclusions address, in turn, the initial numbered objectives posed in Section 1.3:

1. The water table demonstrated dramatic, localized fluctuations, leading to hydraulic gradients as locally high as 0.01. GPR estimates were successfully validated against a succession of measurement wells (error <±15 cm in all cases), and best-fitting sub-surface velocity models that were generated using seismic refraction data.
2. The hydraulic conductivity of the gravels was high and depended non-linearly on gradient; at large (>0.05) gradients, K ~ 0.01–0.04 ms^{-1}, of the same order of magnitude as the estimate from a pumping test (K = 0.010 ms^{-1}).
3. At smaller hydraulic gradients (<0.03), the assumption of linear groundwater flow broke down, which was also observed at field scale.
4. The observed water table fluctuations, lack of a regional head gradient, and the existence of several faster-flow pathways (evidenced by a tracer test, and corroborated by groundwater flow simulations), may be explained by the strong heterogeneity of the gravel aquifer, as well as its sensitivity to the imposition of sub-surface obstacles such as clay-lined backfilled gravel pits, or deep basements. Groundwater levels did not exhibit a strong temporal or spatial dependence on River Thames stage, suggesting a thick hyporheic zone that retards water transfer.
5. An extreme rainfall event at the beginning of January 2024 raised river levels (lag time ~days) and groundwater levels (lag time ~weeks). We identified 65 localities of surface

and basement flooding. These floodwaters were chemically identical to groundwater pumped from the gravel aquifer. Groundwater emergence manifested itself in a series of highly localized patches, independent of the course of surface drainage. Rather, in our simulations, 80% of groundwater flood locations can be explained by hydraulic head, predicted using the variable gravel thickness distribution and taking into account sub-surface flow barriers like clay-lined gravel pits, lying above local surface level.

6. We suggest that aquifer thickness and head variations (i.e. hydraulic gradients) be taken into account in the development of future maps of groundwater flood risk. Current UK practice only exploits sub-surface permeability maps, which (especially for urbanized catchments) do not account for barriers to groundwater flow. Combined with weather prediction ensembles, high-resolution head maps could be leveraged to simulate future water table variations.

The combination of geophysical surveys, hydro(geo)logical tests, laboratory analyses, and citizen science, presented a fruitful approach to tackling this hydrogeological approach: local knowledge was incorporated into survey design, while the laboratory and field analyses were complementary and obviated the scale effect (in the measurement of hydraulic conductivity). The outstanding issues are those of (a) resolution: the work presented here offers a temporal snapshot of one portion of a highly heterogeneous superficial aquifer; and (b) governance. In order to generate the “impact” so often sought by local residents (i.e. reducing the magnitude and effects of groundwater emergence, or at least its mitigation), groundwater flooding must be explicitly investigated, modeled, and presented in risk/vulnerability maps, together with fluvial or sea flooding, by environmental regulators.

Acknowledgments

Quality-related Research (QR) funding is acknowledged from Research England. We are very grateful for fruitful hydrologic discussions with >700 local residents, business owners, and councilors from Staines and environs. Martin Blunt and Peter King, and David Shilston, are thanked for aiding with porous media physics, and geotechnical interpretations and access/aid with the aquifer tests, respectively. We are grateful to Iñaki Valcarcel for the hydrogeochemical laboratory analyses. Finally I am indebted to Nigel Rowe, head of the Riverside Residents (Staines) Coalition, who acted as a key local fixer and social enabler to catalyze local stakeholder

involvement.

Open Research

Metadata related to boreholes, river and groundwater level measurements, GPR surveys, and the location of groundwater emergence are available in the Appendix. Hydrogeochemical data are given in Table 2. UK Lidar DTM data, borehole records of local stratigraphy, and river level time series are available under the Open Government licence respectively from: https://environment.data.gov.uk/survey; https://www.bgs.ac.uk/map-viewers/geoindex-onshore/; and https://nrfa.ceh.ac.uk/data/search.

References

Agarwal R.G., 1980. A new method to account for producing time effects when drawdown type curves are used to analyze buildup and other test data. SPE Paper 9289, *55th SPE Annual Technical Conference and Exhibition*, Dallas, TX

Alexander M., Berg S.J., Illman W.A., 2011. Field study of hydrogeologic characterization methods in a hetereogeneous aquifer. *Groundwater*, 49, 365–382

Allen D.J., Brewerton L.J., Coleby L.M., et al., 1997. The physical properties of the major aquifers in England and Wales. *BGS Technical Report WD/97/34*

Ameen S., Dahi Taleghani A., 2015. Dynamic modeling of channel formation during fluid injection into unconsolidated formations. *SPE Journal*, 20, 689–700

Baird R., Bridgewater L., 2017. *Standard Methods for the Examination of Water and Wastewater*. American Public Health Association, Washington D.C.

Bery A., Saad R., 2012. Correlation of seismic P-wave velocities with engineering parameters (N value and rock quality) for tropical environmental study. *International Journal of Geosciences*, 3(4), 749–757

Birks D., Whittall S., Savill I., Younger P.L., Parkin G., 2013. Groundwater cooling of a large building using a shallow alluvial aquifer in Central London. *Quarterly Journal of Engineering Geology and Hydrogeology*, 46, 189 – 202.

Bloomfield J., 1996. Characterisation of hydrogeologically significant fracture distributions in the Chalk: An example from the Upper Chalk of southern England. *Journal of Hydrology*, 184(3–4), 355–379

Bohling G.C., Anderson M.P., Bentlet C.R., 1989. Use of ground penetrating radar to define recharge areas in the Central Sand Plain. *Technical Completion Report G1458-03*, Geology and Geophysics Department, University of Wisconsin-Madison, Madison, WI.

Buytaert W., Zulkafli Z., Grainger S., Acosta L., Alemia T.C., et al., 2014. Citizen science in hydrology and water resources: Opportunities for knowledge generation, ecosystem service management, and sustainable development. *Frontiers in Earth Science*, 2, 26 pp.

Chontpantarat S., Thamrongsrisakul J., 2021. Natural and anthropogenic factors influencing hydrochemical characteristics and heavy metals in groundwater surrounding a gold mine, Thailand. *Journal of Asian Earth Sciences*, 211, 104692

Defra, Welsh Government, Natural Resources Wales, and Environment Agency, 2020. *Development of Interim National Guidance on Non-Stationary Flood Estimation*. Science Report FRS18087/1G/R1. UK Department for Environment, Food, and Rural Affairs, London.

Ding G., Jiao J.J., Zhang D., 2008. Modelling study on the impact of deep building foundations on the groundwater system. *Hydrological Processes*, 22, 1857–1865

Dochartaigh B.E.O., Archer N.A.L., Peskett L., Macdonald A.M., Black A.R., et al., 2019. Geological structure as a control on floodplain groundwater dynamics. *Hydrogeology Journal*, 27(2), 703–716

Doolittle J.A., Jenkinson B., Hopkins D., Ulmer M., Tuttle W., 2006. Hydropedological investigations with ground-penetrating radar (GPR): Estimating water-table depths and local ground-water flow pattern in areas of coarse-textured soils. *Geoderma*, 131(3–4), 317–329

Duffield G.M., 2007. *AQTESOLV for Windows Version 4.5 User's Guide*. HydroSOLVE Inc., Reston, VA

Ellison R.A., Woods M.A., Allen D.J., Forster A., Pharoah T.C., 2004. *Geology of London*. British Geological Suvey, Keyworth, Nottingham, UK.

Environment Agency (UK EA), 2020. *National Flood and Coastal Erosion Risk Management Strategy for England*. Report CCS0919045990. Bristol, UK: Environment Agency.

Essam D., Ahmed M., Abouelmagd A., Soliman F., 2020. Monitoring temporal variations in groundwater levels in urban areas using ground penetrating radar. *Science of the Total Environment*, 703, 134986.

Fan Y., 2024. Ensemble flood predictions for River Thames under climate change. *National Science Open*, 3(1), 20230027

Feuerstein D.W., Selleck R., 1963. Fluoresecent tracers for dispersion measurements. *Journal of the Sanitation Engineering Division, American Society of Civil Engineers*, 89(SA4), 1–21

Gan Q., Elsworth D., Zhao Y., Grippa A., Hurst A., 2020. Coupled hydro-mechanical evolution of fracture permeability in sand injectite intrusions. *Journal of Rock Mechanics and Geotechnical Engineering*, 12(4), 742–751

Geometrics Inc., and OYO Inc., 2009. SeisImager manual, v. 3.3 [computer program manual]. OYO Corporation, Tokyo, Japan.

Gueting N., Vienken T., Klotzsche A., van der Kruk J., Vanderborght J., Caers J., Vereecken H., Englert A., 2017. High resolution aquifer characterization using crosshole GPR full-waveform tomography: Comparison with direct-push and tracer test data. *Water Resources Research,* 53, 49–72

Jiao J.J., Wang X.S., Nandy S., 2006. Preliminary assessment of the impacts of deep foundations and land reclamation on groundwater flow in a coastal area in Hong Kong, China. *Hydrogeology Journal*, 14, 100–114

Kasanavia T., Vu D., Sabatini D.A., 1999. Fluorescent dye and media properties affecting sorption and tracer selection. *Groundwater*, 37(3), 376–381

Keiswetter D., Steeple D., 1994. Practical modifications to improve the sledgehammer seismic source. *Geophysical Research Letters*, 21(20), 2203–2206

Kim I., Park D., Kyung D., Kim G., Kim S., Lee J., 2016. Comparative influences of precipitation and river stage on groundwater levels in near-river areas. *Sustainability*, 8(1), 1

Konstantinou C., Biscontin G., 2022. Experimental investigation of the effects of porosity, hydraulic conductivity, strength, and flow rate on fluid flow in weakly cemented bio-treated sands. *Hydrology*, 9(11), 190

Larkin R.G., Sharp J.M., 1992. On the relationship between river-basin geomorphology, aquifer hydraulics, and ground-water flow direction in alluvial aquifers. *GSA Bulletin*, 104(12), 1608–1620

Linde-Arias E., Harris D., Ghail R., 2018. Engineering geology and tunnelling in the Limmo Peninsula, East London. *Quarterly Journal of Engineering Geology and Hydrogeology*, 51(1), 23–30

Macdonald D.M.J., Bloomfield J.P., Hughes A.G., Macdonald A.M., Adams B., McKenzie A.A., 2008. Improving the understanding of the risk from groundwater flooding in the UK. *Proceedings of the European Conference on Flood Risk Management*, Oxford, 30 September – 2 October 2008.

Macdonald A., Dixon A., Newell A., Hallaways A., 2012. Groundwater flooding within an urbanized flood plain. *Journal of Flood Risk Management*, 5, 68–80

Maimone M., O'Rourke D.E., Knighton J.O., Thomas C.P., 2011. Potential impacts of extensive stormwater infiltration in Philadelphia. *Environmental Engineer: Applied Research and Practice*, 14.

Malzone J.M., Anseeuw S.K., Lowry C.S., Allen-King R., 2016. Temporal hyporheic zone response to water table fluctuations. *Groundwater*, 54, 274–285

Manga M., 1999. On the timescales charaterising groundwater discharge at springs. *Journal of Hydrology*, 219(1–2), 56–69

Mavroulidou M., Gunn M.J., Woods R.I., 1998. Analysis of pumping from the Deep London Aquifer. *Proceedings of the Third International Conference on Hydrological Science and Engineering*, Cottbus, Berlin.

McKenzie A.A., Rutter H.K., Hulbert A.G., 2010. The use of elevation models to predict areas at risk of groundwater flooding. In: Fleming C., Marsh S.H., Giles J.R.A. (eds.), *Elevation Models for Geoscience.* Geological Society of London, Special Publications, 345, 75–79

Morgan-Jones M., Bennett S., Kinsella J.V., 1984. The hydrological effects of gravel winning in an area west of London, United Kingdom. *Groundwater*, 22, 154–161

Mulqueen J., 2005. The flow of water through gravels. *Irish Journal of Agricultural and Food Research*, 44, 83–94.

Morris S.E., Cobby D., Parkes A., 2007. Towards groundwater flood risk mapping. *Quarterly Journal of Engineering Geology and Hydrogeology*, 40(3), 203–211

Nardi F., Cudennec C., Abrate T., Allouch C., Annis A., et al., 2022. Citizens AND Hydrology (CANDHY): Conceptualising a transdisciplinary framework for citizen science addressing hydrological challenges. *Hydrological Sciences Journal*, 67(16), 2534–2551

Parkin G., 2024. Briefing: Groundwater flooding – A hidden hazard. *Proceedings of the Institution of Civil Engineers*, e-publication ahead of print.

Paul J.D., Buytaert W., Allen S., Ballesteros-Canovas J.A., Bhusal J., et al., 2018. Citizen science for hydrological risk reduction and resilience building. *Wiley Interdisciplinary Reviews: Water*, 5, e1262

Robins N.S., Finch J.W., 2012. Groundwater flood or groundwater-induced flood? *Quarterly Journal of Engineering Geology and Hydrogeology*, 45, 119–122

Roldin M., Locatelli L., Mark O., Mikkelsen P.S., Binning P.J., 2013. A simplified model of soakaway infiltration interaction with a shallow groundwater table. *Journal of Hydrology*, 497, 165–175

Sharma P.V., 1997. Environmental and Engineering Geophysics. Cambridge University Press, Cambridge, UK.

Smart P.L., Laidlaw I.M.S, 1997. An evaluation of some fluorescent dyes for water tracing. *Water Resources Research*, 13(1), 15–33

Smith M.C., Vellidis G., Thomas D.L., Breve M.A., 1992. Measurement of water table fluctuations in a sandy soil using ground penetrating radar. *Transactions of the American Society of Agricultural Engineers*, 35, 1161–1166

South West Suburban Water Company, 1971. *Pumping test at Holm Pit Island, Egham*. Report LJB/D/125, Groundwater Division, London.

Sumbler M.G., 1996. *British Regional Geology: London and the Thames Valley* (4th edition). HSMO for the British Geological Survey, London.

Theis C.V., 1935. The relation between the lowering of the piezometric surface and the rate and duration of discharge of a well using groundwater storage. *Americal Geophysical Union Transactions*, 16, 519–524

Tillard S., Dubois J.-C., 1995. Analysis of GPR data: Wave propagation velocity determination. *Journal of Applied Geophysics*, 33(1–3), 77–91

Van der Veen M., Buness H.A., Bueker F., 2000. Field comparison of high-frequency seismic sources for imagine shallow (10–250 m) structures. *Journal of Environmental and Engineering Geophysics*, 5(2), 1–58

Van Overmeeren R.A., 2004. Georadar for hydrogeology. *Fastbreak*, 12, 401–408

Welch C., Harrington G.A., Leblanc M., Batlle-Aguilar J., Cook P.G., 2014. Relative rates of solute and pressure propagation into heterogeneous alluvial aquifers following river flow events. *Journal of Hydrology*, 511, 891–903

Wilson I., 1984. The effects of gravel extraction on groundwater hydrology. PhD dissertation, University of Oxford

Wondzell S.M., Swanson F.J., 1999. Floods, channel changes, and the hyporheic zone. *Water Resources Research*, 35(2), 555–567

World Health Organisation (WHO), 2011. *Guidelines for drinking-water quality*, 4th edition. WHO Press: Geneva, Switzerland.

Xayavong V., Duc Vu M., Anh Duong N., Minh Tuan V., 2020. Seismic refraction exploration for groundwater potential evaluations: A case study of Vientiane Province, Laos. *VNU Journal of Science: Earth and Environmental Sciences*, 36(4), 90–101

Xiao J., Wang L., Deng L., Jin Z., 2019. Characteristics, sources, water quality and health risk assessment of trace elements in river water and well water in the Chinese Loess Plateau. *Science of the Total Environment*, 650(2), 2004–2012

Yordkayhun S., Na Suwan J., 2012. A university-developed seismic source for shallow seismic surveys. *Journal of Applied Geophysics*, 82, 110–118

Appendix

Table A1. Location and description of river and groundwater level gauges, rain gauges, and seismic refraction surveys (January 7 2024).

ID	Eastings	Northings	Elev / m	Description
2900TH	503520	171340	10	EA River level - RThames at Staines
2901TH	504429	169458	12.56	EA River level - RThames at Penton Hook
3115TH	504608	171287	13	EA River level - R Ash at Knowle Green
-	503708	169960	13.82	7 Jan 24 - seismic refraction survey - Wheatsheaf Ln field
-	504326	170669	13.9	7 Jan 24 - seismic refraction survey - Staines Park
-	504368	170732	14.06	Rain gauge and groundwater level monitoring point – deployed as part of this project - Staines Park

Table A2. Location and description of boreholes drilled as part of this project, from which gravel was extracted and groundwater level measured on 7 January 2024 (N = 10).

ID	Eastings	Northings	Water table / mAOD	Description

BH1	503483	171252	14.72	This project borehole - Staines Boat Club
BH2	504582	171234	14.17	This project borehole - Knowle Green
BH3	504444	169663	13	This project borehole - Penton Hook Farm
BH4	502703	171885	14.61	This project borehole - Lammas Rec
BH5	505099	172085	14.59	This project borehole - Shortwood Common
BH6	502343	171217	14.22	This project borehole - Hythe Park
BH7	503657	170080	14.74	This project borehole - Wheatsheaf Ln field
BH8	505517	170756	13.53	This project borehole - Matthew Arnold School playing fields
BH9	502759	169472	26.06	This project borehole - SW Egham Hythe field
BH10	504643	168705	13.52	This project borehole - Penton Park

Table A3. Location and description of verified resident-provided groundwater flooding, January 2024 (N = 65); residential/industrial gravel aquifer groundwater pumping sites (N = 37); buildings whose basements extend through the gravel into the underlying London clay (N = 5); and former gravel pits that are now backfilled (N = 9). Some precise locations have been redacted ("X") at the request of local residents and/or local government. * = water sampled for hydrochemical analyses (Table 2; Figure 7). ** = tube wells for pumping test.

ID	Eastings	Northings	Description
FORMER GRAVEL PITS			
GP1	503757	171326	Staines central
GP2	503823	171110	Gresham Rd
GP3	504159	170382	Laleham Rd
GP4	503135	169791	Egham Hythe
GP5	505528	169732	Ashford Rd
GP6	504582	169916	Staines Rd
GP7	504364	170805	Staines Park W
GP8	504015	169995	Avondale Ave
GP9	503496	170665	Chertsey Ln/Bundy's Way
DEEP-BASEMENT TALL BUILDINGS			
BLDG1	503743	171785	X
BLDG2	504014	171822	X
BLDG3	503830	171759	X
BLDG4	503626	171441	X
BLDG5	503655	171390	X
GROUNDWATER FLOODING JAN 2024			
FLD1	504156	170890	Riverbridge Primary Sch
FLD2	504078	170707	Guildford St
FLD3	504334	170585	Parkside Pl
FLD4	504543	169653	The Ryde

FLD5	504448	170288	Grosvenor Rd 1
FLD6	504430	170462	Grosvenor Rd 2
FLD7	504184	170159	X Wheatsheaf Ln
FLD8	504285	170172	X Wheatsheaf
FLD9	503828	170138	X pub
FLD10	503511	171549	Old Debenhams
FLD11*	503264	171565	X
FLD12	502977	171719	Church Island
FLD13	503789	171276	X Richmond Rd
FLD14	501832	171602	Glanty
FLD15	502235	171656	ADP office block
FLD16*	502582	171493	Chandos Rd
FLD17	502691	171550	Claremont Rd
FLD18	502509	171558	X The Causeway
FLD19	504187	170570	Broomfield
FLD20	502152	170824	Egham Town Football Club
FLD21	504321	170499	X Parkside Pl
FLD22	504470	170227	X Florence Gardens
FLD23	504360	169779	X
FLD24	504572	169552	X The Ryde
FLD25	504070	171142	X Edgell Rd
FLD26	503964	171273	X/Sweeps Ditch
FLD27	503413	171263	Riverside Drive
FLD28	503254	171386	Opp Swan Hotel, The Hythe
FLD29	503420	171881	TK Maxx car park
FLD30	503608	172107	Plover Cl
FLD31	504120	172086	Staines RWPS
FLD32	504325	171796	X Sidney Rd
FLD33	504367	171701	X Greenlands Rd
FLD34*	504293	171503	Kingston Rd/Greenland Rd
FLD35	502738	171892	Lammas rec
FLD36	502915	171842	Lammas playground/tennis courts
FLD37	502897	171496	Sainsburys A308
FLD38	503512	170877	X Chertsey Ln
FLD39	503463	171015	X Chertsey Ln
FLD40	503477	170252	X Chertsey Ln
FLD41	503478	170372	X Chertsey Ln
FLD42	503894	172036	Aspen Cl car park
FLD43	504162	171362	X car park
FLD44	504145	170962	X Burges Way
FLD45	504148	170835	Lady of the Rosary Primary Sch
FLD46	504215	169923	St Pinnock Ave (multiple props)

FLD47	503442	171079	X Chertsey Ln
FLD48	503275	171764	Staines Travelodge
FLD49	504293	170570	X Octavia Way
FLD50	504364	171044	Staines Park tennis courts
FLD51	503749	170118	X Wheatsheaf Ln
FLD52	503639	170090	Wheatsheaf field NW
FLD53	504466	171623	X
FLD54	503639	169885	Riverside Cl
FLD55*	504229	169711	Penton Hook Rd S
FLD56	504533	171902	Shortwood Common W
FLD57	504706	171584	X Leacroft
FLD58	503869	169941	X Penton Ave
FLD59	503452	169994	X Chertsey Ln
FLD60	504586	169489	X Thamesgate
FLD61	504625	170683	X Commercial Rd
FLD62	504632	170853	X Withygate Ave
FLD63	504639	170916	X Gordon Close
FLD64	504781	170641	Worple Rd/Hurstdene Ave
FLD65	504848	170881	X Worple Ave
PUMPING FROM GRAVEL AQUIFER			
PP1*	503968	170891	X Park Ave
PP2	503980	170902	X Park Ave
PP3**	504330	170800	Allotments Commercial Rd 1
PP4**	504250	170700	Allotments Commercial Rd 2
PP5*	504000	170120	Wheatsheaf Ln
PP6	504790	169700	Notcutts Garden Cr
PP7	502900	170800	Hythe Farm
PP8	503290	169900	Davids Haven
PP9	502900	171200	Eastbridge Thorpe Rd
PP10	503100	171200	X Goring Rd
PP11	503200	171200	X Goring Rd
PP12	501770	171280	Vicarage Rd
PP13	503160	172260	Allotments Moor Ln
PP14	504470	171380	Cattleyard
PP15	505020	171340	Shortwood S Allotments 1
PP16	505170	171240	Shortwood S Allotments 2
PP17	505030	171250	Shortwood S Allotments 3
PP18	504940	171300	Shortwood S Allotments 4
PP19	505110	171800	Shortwood E Allotments 1
PP20	504990	171840	Shortwood E Allotments 2
PP21	505080	171840	Shortwood E Allotments 3
PP22	502900	170300	Devils Lane
PP23	503030	170240	Chertsey Land

PP24	502140	170500	Marston Nursery
PP25	502382	170800	Pooley Green Rec
PP26	502300	171280	Hythe Park
PP27	503442	169655	Egham Hythe
PP28	503562	170588	Chertsey Ln
PP29	503184	172082	Moor Ln
PP30	503880	170648	Jamnagar Cl
PP31	503883	170362	Avondale Ave/Ruskin Rd
PP32	504092	170065	Garrick Cl
PP33	503996	169839	River Rd
PP34	504632	170404	Nursery Gardens SW
PP35	502908	172104	Field to E of Lammas Lake
PP36	504343	171217	Spelthorne Leisure Centre
PP37	504530	170022	Laleham Rd / Sweeps Ditch

Table A4. Location and description of boreholes (N = 83) from which stratigraphic logs were extracted (Fig. 1b) via the British Geological Survey (BGS) GeoIndex database.

BGS ID	Eastings	Northings	Elev / m	Base gravel depth / m
TQ07SW149	502000	171980	14.85	6.25
TQ07SW362	502230	172890	14.23	7.3
TQ07SW19	501700	172220	16.13	3.3
TQ07SW143	501810	171780	16.38	5.1
TQ07SW116	501660	171390	15.76	3
TQ07SW185	500850	171310	16.6	4.15
TQ07SW5N5	501120	170700	16.3	2.1
TQ07SW190	501560	170940	17.2	4.3
TQ07SW451	501250	170170	15.84	2.2
TQ07SW132	501590	170380	14.1	2.03
TQ06NW401	500790	169650	14.96	4.1
TQ06NW629	501000	169360	16.16	3.9
TQ06NW781	500900	168880	16.31	1.6
TQ06NW648	501230	168510	13.74	3.3
TQ06NW642	501350	168870	13.66	1.8
TQ06NW26	501660	168340	14.55	2.66
TQ06NW12	501650	169370	14.68	1.98
TQ06NW6	501650	169750	14.9	1.7
TQ06NW640	501960	169590	16.43	2.5
TW06NW625	501810	169980	16.18	1.9
TQ06NW771	502040	168510	14.4	2.75
TQ06NW503	501890	169100	15.83	2.15
TQ06NW558	502550	168660	12.64	5.33

TQ06NW505	502560	169210	20.52	5.1
TQ06NW506	502400	169030	14.53	4.99
TQ06NW650	502620	169540	18.02	3.2
TQ06NW555	503240	168550	12.56	6.33
TQ06NW510	502850	169080	17.05	8
TQ06NW346	503920	168490	13.13	7.33
TQ06NW2/A-H	504300	168700	13.58	9.67
TQ06NW560	503610	168890	14.48	6
TQ06NW776	503390	169280	14.85	7.25
TQ06NW615	503620	169190	13.84	7.9
TQ06NW616	504000	169100	11.57	8.5
TQ06NW711	504960	168790	13.06	10.1
TQ06NE495	505260	168940	13.44	10.4
TQ06NE545	505710	169640	14.43	11
TQ06NE33	505590	169980	14.36	11.3
TQ06NW654	504790	169700	14.18	8.9
TQ06NE647	506030	169960	14.57	9.33
TQ07SE22	505970	170330	14.98	9.5
TQ07SE23	506110	170520	14.94	14.3
TQ07SE324	506090	170840	13.54	12.4
TQ07SE211	506730	171200	14.6	10
TQ07SE332	506090	171780	14.33	12.25
TQ07SE14	505700	171600	14.19	9
TQ07SE364	505040	171580	14.3	9.5
TQ07SW145	504570	172080	14.92	7.33
TQ07SW448	504470	171380	14.08	7
TQ07SW449	504910	171180	14.25	8.33
TQ07SW436	504250	170700	14.2	2.9
TQ07SW454	504400	170610	13.68	10.55
TQ07SW32	504000	170120	13.92	2.1
TQ06NW779	503190	169830	13.92	7.5
TQ06NW508	502510	169880	15.36	6.33
TQ07SW530	502450	170160	13.04	5.25
TQ07SW531	502560	170340	14.2	5.25
TQ07SW227	502900	170300	13.54	6.33
TQ07SW214	503190	170180	14	5.75
TQ07SW228	503320	170450	14.13	6.33
TQ07SW618	502140	170500	14.78	2.9
TQ07SW533	502430	170790	15.65	2.5
TQ07SW534	502730	170940	14.91	2
TQ07SW229	502900	170800	15	4.5
TQ07SW234	503040	171320	17	4.66

TQ07SW425	503200	171200	14.78	4
TQ07SW223	503230	171750	18.33	6.33
TQ07SW204	503470	171460	15.5	8.8
TQ07SW195	503640	171380	15.37	6.85
TQ07SW241	503950	171610	15.41	11
TW07SW152	503900	171800	15.35	7.85
TQ07SW107	504250	172210	15.09	7
TQ07SW230	503640	171980	15	12
TQ07SW28	503200	172170	15.67	7.17
TQ07SW156	503600	172500	15.99	9.9
TQ07SW183	502260	171850	15.29	5.83
TQ07SW235	502480	171720	15.24	4.17
TQ07SW456	502300	172100	13.32	5.5
TQ07SW458	502691	171988	14.62	4.2
TQ07SW182	503030	172270	15.5	9.15
TQ07SW176	503160	172470	16	9.6
TQ07SW174	502760	172580	15.5	9.35
TQ07SW5	502590	173100	18.53	9.67

Table A5. Location and description of GPR spot measurements (N = 141) of water table level, January 7 2024.

ID	Eastings	Northings	Water table / mAOD
GPR1	502741	171561	15.92
GPR2	502980	171491	15.66
GPR3	503096	171423	16.84
GPR4	503012	171303	15.96
GPR5	503162	171323	15.63
GPR6	503286	171235	14.99
GPR7	503384	171129	14.78
GPR8	503452	171039	14.43
GPR9	503494	170923	14.42
GPR10	503530	170743	14.31
GPR11	503510	170568	14.1
GPR12	503476	170412	14.12
GPR13	503472	170164	14.43
GPR14	503442	169714	14.23
GPR15	503536	169495	13.92
GPR16	503678	169281	13.91
GPR17	503720	169203	14.16
GPR18	502941	171174	15.24
GPR19	503198	171597	14.96

GPR20	503292	171689	15.47
GPR21	503302	171733	15.71
GPR22	503280	171832	15.52
GPR23	503230	171884	15.89
GPR24	503136	171926	16.39
GPR25	503348	171641	15.66
GPR26	503380	171597	15.92
GPR27	503454	171555	16.91
GPR28	503498	171523	16.38
GPR29	503548	171441	15.31
GPR30	503606	171347	15.39
GPR31	503634	171273	15.32
GPR32	503680	171163	15.21
GPR33	503738	171093	15.37
GPR34	503850	170943	15.38
GPR35	503926	170829	15.28
GPR36	503981	170678	15.4
GPR37	503964	170614	14.88
GPR38	503944	170486	14.79
GPR39	503934	170440	14.89
GPR40	504031	170454	14.65
GPR41	503926	170290	15.3
GPR42	503938	170158	14.13
GPR43	503916	170130	14.04
GPR44	503832	170112	14.81
GPR45	503802	170192	14.67
GPR46	503818	170026	14.61
GPR47	503724	170094	14.7
GPR48	503670	170004	14.71
GPR49	503944	170058	14.14
GPR50	503952	169996	14.21
GPR51	503968	169892	14.72
GPR52	504025	170154	13.83
GPR53	504167	170180	13.55
GPR54	504263	170198	13.87
GPR55	504353	170218	14.26
GPR56	504147	170100	13.96
GPR57	504185	169966	14.52
GPR58	504207	169844	14.7
GPR59	504273	169986	13.88
GPR60	504337	170000	13.77
GPR61	504385	169892	13.6
GPR62	504295	170114	13.75

GPR63	504917	169319	13.84
GPR64	504829	169463	13.69
GPR65	504745	169640	13.86
GPR66	504709	169730	14.38
GPR67	504653	169848	14.65
GPR68	504565	170002	14.82
GPR69	504515	170086	14.61
GPR70	504427	170164	14.16
GPR71	504315	170296	14.07
GPR72	504225	170376	14.17
GPR73	504151	170480	14.74
GPR74	504103	170552	14.73
GPR75	504705	169930	14.81
GPR76	504717	170068	15.05
GPR77	504725	170150	15.11
GPR78	504739	170262	15.09
GPR79	504783	170384	14.76
GPR80	504801	170446	14.87
GPR81	504791	170546	14.94
GPR82	504775	170628	15.17
GPR83	504761	170707	15.36
GPR84	504657	170691	14.64
GPR85	504567	170685	14.14
GPR86	504457	170674	13.93
GPR87	504355	170660	14.08
GPR88	504221	170644	14.17
GPR89	504113	170630	14.34
GPR90	504751	170805	15.38
GPR91	504743	170891	15.23
GPR92	504765	171023	14.63
GPR93	504839	170999	14.44
GPR94	504931	170967	14.55
GPR95	504703	171065	14.47
GPR96	504641	171125	14.65
GPR97	504575	171183	14.81
GPR98	504489	171127	14.69
GPR99	504409	171093	14.47
GPR100	504281	171115	13.88
GPR101	504179	171159	14.03
GPR102	504109	171219	14
GPR103	503992	171121	14.7
GPR104	503894	171047	15.18
GPR105	504531	171259	14.95

GPR106	504465	171347	17.93
GPR107	504403	171431	19.71
GPR108	504329	171479	16.96
GPR109	504249	171503	15.26
GPR110	504161	171553	15.08
GPR111	504057	171645	15.28
GPR112	503966	171729	15.48
GPR113	504015	171782	15.28
GPR114	504071	171806	15.56
GPR115	504175	171856	15.05
GPR116	503914	171741	15.54
GPR117	503804	171729	15.43
GPR118	503704	171713	15.52
GPR119	503574	171701	15.74
GPR120	503626	171627	16.18
GPR121	503530	171577	17.13
GPR122	503656	171782	15.65
GPR123	503592	171854	15.8
GPR124	503518	171866	15.68
GPR125	503466	171806	16.41
GPR126	503398	171725	15.74
GPR127	503430	171920	15.95
GPR128	503594	171049	15.07
GPR129	503650	171491	14.79
GPR130	504139	171423	16.93
GPR131	503874	171887	15.41
GPR132	504385	170827	14.17
GPR133	504460	170465	13.85
GPR134	504029	169669	15.45
GPR135	504177	169464	15.76
GPR136	503926	171371	14.37
GPR137	503376	171449	15.49
GPR138	503434	169930	14.4
GPR139	504194	169675	14.49
GPR140	503703	169832	14.18

Table A6. Location and description of injection and monitoring boreholes (N = 18) for fluorescein groundwater tracer tests on January 7 2024.

ID	Eastings	Northings	Elev / m	Tracer peak / min	Tracer peak / hr	Description
TR1	503725	171227	12.93	308	5.1	Tracer BH - Gresham Rd
TR2	503198	171674	12.87	1059	17.7	Tracer BH - Bridge St Car Park

TR3	502871	170673	12.9	1722	28.7	Tracer BH - Bishops Way Rec
TR4	503786	170266	12.75	1392	23.2	Tracer BH - Wheatsheaf Lane field
TR5	504386	169598	11.78	1110	18.5	Tracer BH - N Penton Hook Lock
TR6	504491	170094	13.56	1299	21.7	Tracer BH - Laleham Rd / Sweeps Ditch
TR7	504505	170832	13.03	488	8.1	Tracer BH - Sweeps Ditch at Staines Park
TR8	504002	171259	14.18	0	0.0	INJECTION Tracer BH - Sweeps Ditch at Staines railway station
TR9	503058	169676	12.94	2000	33.3	Tracer BH - Mead Lake at Egham Hythe
TR10	503485	171852	13.49	1980	33.0	Tracer BH - Wraysbury at A30 bridge
TR11	504262	171931	15.13	1051	17.5	Tracer BH - Colne at A30 bridge
TR12	505047	170433	15.45	1342	22.4	Tracer BH - Berryscroft Court
TR13	502703	171885	14.61	1438	24.0	Tracer BH (=BH4) - Lammas Rec
TR14	504079	170359	14.79	725	12.1	Tracer BH - Meadway
TR15	503605	171581	13.15	1887	31.5	Tracer BH - Elmsleigh Rd
TR16	502978	171247	15.31	1550	25.8	Tracer BH - Wendover Rd
TR17	503483	171252	14.72	611	10.2	BH1 - This project borehole - Staines Boat Club
TR18	504582	171234	14.17	1291	21.5	BH2 - This project borehole - Knowle Green